GEORG-AUGUST-UNIVERSITÄT
GÖTTINGEN

Master's Thesis

Dynamik des ribosomalen Ausgangstunnels

Dynamics of the ribosomal exit tunnel

prepared by

Vitali Telezki

from Shambyl (Kazakhstan)

at the Max Planck Institute for Biophysical Chemistry

Thesis period: 14th July 2017 until 5th December 2017

First referee: Prof. Dr. Helmut Grubmüller

Second referee: Prof. Dr. Tim Salditt

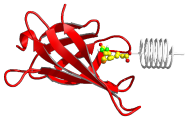

Zusammenfassung

Die vorliegende Masterarbeit beschäftigt sich mit der Dynamik des ribosomalen Ausgangstunnels und der Fragestellung, wie diese von der Anwesenheit des im Ribosom synthetisierten Proteins beeinflusst wird: Zum einen scheinen besonders die Schleifen der ribosomalen Proteine von der Answesenheit einer Peptidkette beeinflusst zu sein. Zum anderen steigt die Flexibilität der rRNA zum Ende des Tunnels unabhängig von der Anwesenheit einer Peptidkette an. Diese Eigenschaft eröffnet die Frage, ob es sich dabei um einen möglichen Mechanismus handelt, der das Peptid bei dem Verlassen des Tunnels unterstützt.

Stichwörter: Physik, Molekulardynamik Simulationen, *E. Coli*, Ribosom, Ribosomaler Ausganstunnel, Dynamik, PCA, nascent chain, RMSD, RMSF.

Abstract

This thesis investigates the dynamics of the ribosomal exit tunnel and how they are affected by the presence of nascent chains. All-atom molecular dynamics simulations were analyzed. Principal component analysis revealed that the conformations of the exit tunnel are affected by the presence of a nascent peptide. Furthermore, investigation of the mobility of the ribosomal exit tunnel indicates that the protein loops seem to be especially affected by the nascent peptide. In addition, the flexibility of the rRNA behind the constriction site increases. This increase seems to be independent of the presence of a nascent chain. This features raises the question whether a possible guidance mechanism of the tunnel regarding the emerging peptide exists.

Keywords: physics, molecular dynamics simulations, *E. Coli*, ribosome, ribosomal exit tunnel, dynamics, PCA, nascent chain, RMSD, RMSF.

Contents

Nomenclature

Symbols

Vectors are denoted by small, bold italic letters $\boldsymbol{v}$. Matrices are denoted by capital, bold italic letters $\boldsymbol{M}$.

Residue numbering and proteins

Residues are numbered according to *E. Coli* numbering if not otherwise specified. Additionally, the nomenclature for protein naming as proposed by Ban et al. [7] is applied.

Abbreviations

Abbreviation	**Meaning**
A-site	aminoacyl-site
cryo-EM	cryo-electron microscopy
E. Coli	*Escherichia coli*
ERY	erythromicin
E-site	empty-site
MD	molecular dynamics
mRNA	messenger ribonucleic acid
PDB	Protein Data Bank
P-site	peptidyl-site
PTC	peptidyl transferase center
RNA	ribonucleic acid
rRNA	ribosomal ribonucleic acid
SecM	secretion monitor

Abbreviation	**Meaning**
tRNA	transfer ribonucleic acid
VemP	Vibrio export monitoring polypeptide

1 Introduction

Ribosomes are found in every living cell. They synthesize proteins and are therefore essential for the organism. Proteins are synthesized deep inside the ribosome at the peptidyl transferase center (PTC). From here the newly synthesized protein leaves the ribosome via the ribosomal exit tunnel. Although many details of protein synthesis are well understood, little is known about the role and impact of the dynamics of the ribosomal exit tunnel on protein synthesis.

In the middle of the 20th century, ribosomes were merely seen as a collection of ribonucleic acid (RNA) rich particles in the cell [46, 60]. At the end of the 20th century it was discovered that ribosomes synthesize proteins [45]. This discovery was mostly driven by improved microscopy. Cryo-electron microscopy (cryo-EM) imaging and X-ray crystallography gave access to more accurate substructures. This led us to better understand the structure and function of ribosomes, currently with a resolution of up to 2.1 Å [44].

This thesis investigates the dynamics of the ribosomal exit tunnel and addresses the following main questions.

- What are the dominant modes of motion of the ribosomal exit tunnel?
- Are the modes of motion affected by the nascent chain and if so, how?
- Does the nascent chain affect the mobility of the exit tunnel?

To find answers to these questions, all-atom molecular dynamics (MD) simulations of the prokaryotic *Escherichia coli* (*E. coli*) ribosome with and without the stalling peptides ErmBL and TnaC inside the ribosomal exit tunnel were analyzed.

In the following, I will first present the current state of research regarding ribosomes and peptide synthesis.

1.1 Ribosomes

Ribosomes are macromolecular complexes. They translate genetic information encoded in the messenger RNA (mRNA). As shown in Figure 1.1, all ribosomes are composed of two subunits; the small (dark green) and the large (light green) subunit, denoted as 30S and 50S subunit for prokaryotes. Both subunits consist of RNA and proteins. The mass ratio between RNA and proteins is roughly two to one in prokaryotic ribosomes. The small and the large subunit of the *E. coli* ribosome contain 21 and 34 different proteins, respectively [3]. Upon initiating translation, the two subunits associate to form a functional ribosome, denoted as 70S. The complete prokaryotic ribosome is approximately 200 Å to 250 Å in diameter and weighs about 2.6 MDa to 2.8 MDa [41].

Transfer RNA (tRNA) translates information encoded in the mRNA in the following way. An anticodon is located on the one side of the tRNA. This anticodon is complementary to the mRNA that progresses through the ribosome during translation. The anticodon is formed by three RNA bases. The corresponding amino acid is located on the other side of the tRNA, ready to be polymerized into a polypeptide. The binding sites for incoming tRNA are located at the interface between both subunits. The ribosome has three binding sites for tRNA. The A-site (aminoacyl), the P-site (peptidyl) and the E-site (exit), between which the tRNA is translocated during peptide synthesis [51].

The amino acids are polymerized at the PTC (dark grey) [19]. The newly synthesized polypeptide, also known as nascent chain, leaves the ribosome through the ribosomal exit tunnel (light grey) which is embedded in the large subunit.

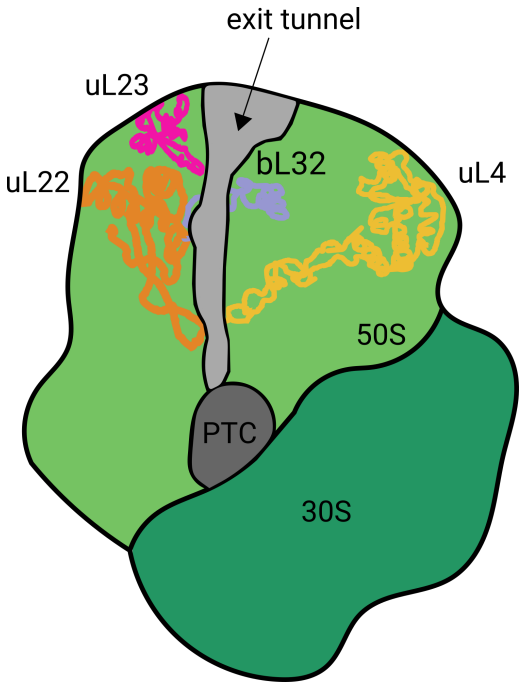

Figure 1.1: Scetch of a prokaryotic ribosome with the small (30S, dark green) and large (50S, light green) subunits. The ribosomal exit tunnel (light grey) is located within the 50S subunit, starting from the PTC (dim grey). The trace of four ribosomal proteins of the 50S subunit is depicted. The proteins uL4 (yellow), uL22 (orange) and uL23 (magenta) are mostly located on the surface of the ribosome. While proteins uL23 and bL32 (grey-blue) are found close to the exit of the tunnel, uL4 and uL22 reach deep inside the 50S subunit and constrict the exit tunnel close to the PTC.

Because of the wealth of structures [5, 6, 12, 17, 28, 33, 44, 54, 62], I will focus on the prokaryotic ribosomes of *E. coli* in this thesis.

1.2 Ribosomal exit tunnel

The first electron microscopy images of the ribosomal exit tunnel were obtained by Milligan et al. in 1982 [38]. The tunnel starts at the PTC and is approximately

100 Å long [8]. Depending on the secondary structure of the polypeptide chain, the tunnel can accommodate a 30 (extended) to 40 (α-helix) residue long chain [59]. The diameter of the tunnel varies between 10 Å and 20 Å along the tunnel axis [42].

High-resolution crystal structures show that the tunnel is porous for small molecules, such as water [30]. The exit tunnel is mainly composed of nucleotides of the 23S ribosomal RNA (rRNA), which is part of the 50S subunit. The narrowest part, also known as the constriction site, is located about 30 Å away from the PTC. This constriction is formed by the uL4 and uL22 proteins of the large subunit. The tunnel wall is mostly, but not uniformly, negatively charged and is thus hydrophilic [34].

Every synthesized peptide has to emerge via the exit tunnel. This raises the question if and how the tunnel walls interact with the emerging peptide. So far, only few interactions are known. Most experimental results are currently limited to a special kind of peptide chain, the so called stalling sequence. The elongation process is stalled in a distinct state during the translation of these sequences. Therefore, it becomes possible to reconstruct the nascent chain inside the ribosome from cryo-EM densities. Due to the intrinsic heterogeneity of the translation states, the reconstruction of non-stalling peptides inside the ribosome is currently not possible.

1.3 Stalling sequences

Stalling is an important regulatory mechanism of protein synthesis at the translation level. Based on cryo-EM reconstruction, it was proposed that specific amino acids of the emerging peptide contact special sensory nucleotides of the ribosomal exit tunnel walls, causing translational arrest [35]. Furthermore, in some cases stalling is especially sensitive to antibiotics [6, 27].

15 cryo-EM structures of *E. Coli* ribosomes including nascent chains were resolved at a resolution of 4.0 Å or higher. Based on this, the impact of the arresting peptides

ErmBL, ErmCL, SecM, TnaC and VemP on the dynamics of the ribosomal exit tunnel was analyzed in this thesis. These peptides do not only differ in the number of amino acids. They also differ in their position inside the ribosomal exit tunnel, their interactions with the exit tunnel and thus their stalling mechanisms.

1.3.1 ErmBL

ErmBL acts as a sensor for the presence of the antibiotic erythromycin (ERY). The peptide chain contains 17 amino acids. The ErmBL peptide barely reaches the uL4 and uL22 constriction with its N-terminal (Fig. 1.2, A). Translational stalling occurs in the presence of the macrolide antibiotic erythromycin (not shown). Due to the arrest, a downstream gene on the mRNA is exposed. Translation of this gene leads to methylation of a nucleotide in the binding site of ERY. This process prevents the binding of the antibiotic on the ribosomal exit tunnel and leads to antibiotic resistance of the organism. It is essential for the organism that methylation of this nucleotide only happens in the presence of the antibiotic [20].

The presence of the antibiotic induces a conformational change of the ErmBL peptide. Due to steric occlusion the P-site tRNA A76 is displaced. Both conformational changes combined perturb peptide-bond formation by increasing the distance between the P-site tRNA residue Asp10 and the A-site tRNA residue Lys11 [6]. The perturbation indicates that conformational dynamics of the ribosomal exit tunnel are functionally relevant.

The altered conformation of the ErmBL peptide allows an interaction between Arg7 and 23S rRNA nucleotides of the tunnel wall [6]. This interaction shows that the presence of a stalled peptide affects the conformation of rRNA.

1.3.2 ErmCL

ErmCL contains 9 amino acids and is the shortest peptide analyzed in this thesis. Similar to the ErmBL peptide, stalling occurs in the presence of an antibiotic, such as erythromycin. Complex interactions between the peptide, the sugar of erythromycin and the ribosomal tunnel walls prevent further peptide-bond formation [61]. Stalling does not occur if the 23S rRNA nucleotides A2503 or A2062 are mutated [56, 58]. Mutational analysis indicates that specific rRNA residues are functionally relevant.

1.3.3 TnaC

The TnaC leader peptide contains 24 residues and regulates the synthesis and degradation of tryptophan. This regulation depends on whether tryptophan needs to be used as a source of carbon, nitrogen and energy [24]. TnaC is almost twice as long as the ErmBL peptide. The N-terminus of TnaC is located close to the loop of the uL23 protein (Fig. 1.2, B).

Stalling is sensitive to the free tryptophan levels in the cell. The peptide is translated and the mRNA is released from the ribosome at low levels of tryptophan. At high levels of free tryptophan, however, translation stalls. Stalling enables the transcription of a downstream gene on the mRNA [52]. Tryptophanase (*tna*A) and tryptophan permease (*tna*B) are then translated. Both enzymes are needed to reduce the levels of free tryptophan in the cell.

Genetic and biochemical analysis show that the TnaC residues W12 [15] and I19 [36] are essential for stalling to occur. Furthermore, interactions with the rRNA nucleotide A2058 contribute to the stalling of the synthesis [36]. The contribution to stalling shows that specific tunnel peptide interactions are functionally relevant.

1.3.4 SecM

Translational stalling of SecM is used to regulate the secretion pathway. This pathway is used to export proteins into the periplasm of the cell [37, 39]. The protein is 170 amino acids long and contains a stalling sequence of 17 amino acids [62]. SecM is the longest peptide analyzed in this thesis (Fig. 1.2, C).

It was shown that mutations of rRNA nucleotides (A2062, A2085 or A2503), as well as mutation or deletion of selected protein residues of the constriction site mitigate stalling to different extents [31, 40, 56]. These results suggest that not only selected rRNA residues but also selected ribosomal proteins are functionally relevant.

1.3.5 VemP

Stalling of the VemP peptide enables the bacterium *Vibrio alginolyticus* to adapt to changes in salt concentration which allows the organism to survive low salinity [26].

VemP contains 37 amino acids. Unlike the nascent chains mentioned above, VemP is extremely compact. The peptide forms two α-helices connected by an α-turn and a loop (Fig. 1.2, D). The compactness allows the nascent chain to be located within the first 50 Å to 55 Å of the ribosomal exit tunnel. The first α-helix starts directly at the PTC of the ribosome and contains the first ten amino acids. The second α-helix is located behind the constriction site and also contains ten amino acids [54].

Mutagenesis scanning identified ten peptide residues that are critical for stalling, from which many interact with the ribosomal exit tunnel. The hairpin of the uL22 protein and 23S nucleotides contribute to the efficiency of the stalling process [26, 54]. This result suggest that selected protein and rRNA residues of the exit tunnel are functionally relevant.

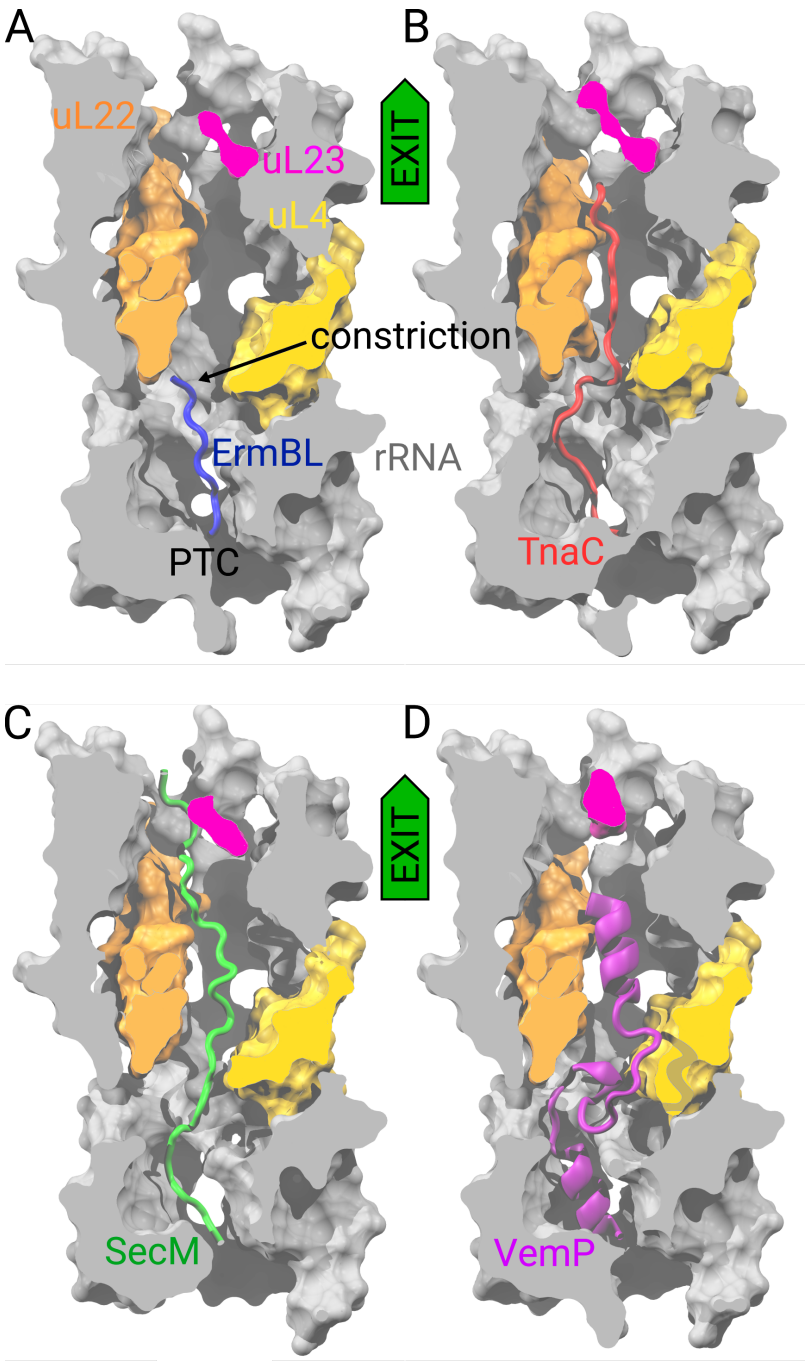

Figure 1.2: Structure of four nascent chains inside the ribosomal exit tunnel as observed by cryo-EM. The tunnel consists mainly of ribosomal RNA (grey). Proteins uL4 (yellow), uL22 (orange) and uL23 (magenta) are visible in the clipped plane. **A** ErmBL (blue) [6] is the shortest peptide. It barely reaches the constriction site made by uL4 and uL22. **B** TnaC (red) [12] is the second longest peptide, it almost reaches protein uL23. **C** SecM (green) [62] is the longest peptide. It reaches protein uL23. **D** VemP (purple) [54] adapts a secondary structure inside the tunnel. With its two α-helices, VemP occupies more than half of the ribosomal exit tunnel.

2 Methods

In this section, I will first present how the exit tunnel was defined in the present study. Then I will list and explain the methods that were used to describe the structure and the dynamics of the ribosomal exit tunnel.

2.1 Defining the ribosomal exit tunnel

To define the ribosomal exit tunnel less sensitive to the choice of a reference frame, tunnel residues were selected based on their solvent-accessible surface area (SASA).

To capture possible conformational changes of the tunnel walls, 15 structures obtained by cryo-EM and one by X-ray crystallography (Tab. 2.1) were used to define the tunnel residues. The following steps were applied to every experimental structure [1]. Present nascent chains or antibiotics were ignored during the definition of the ribosomal exit tunnel.

The SASA of atoms was calculated within a cylindrical volume with a radius of 15 Å (Fig. 2.1). The axis of the cylindrical volume (blue dashed box) is described by the tunnel axis (red line). The tunnel axis was defined by the center of mass of the following selected residues. Residues A2602 and U2585 of the 23S stalk defined the center of mass of the PTC (COM PTC). Residues 46, 52 and 61 of protein uL24

[1] The structures are available at the protein data bank (PDB). The PDB archive serves as a globally accessible repository for structures of proteins, nucleic acids and complex assemblies [11].

PDB ID	Nascent Chain	Resolution	Published by
5JTE	ErmBL	3.6 Å	Arenz et al. [6]
5JU8	ErmBL	3.6 Å	Arenz et al. [6]
5L3P	ErmCL	3.7 Å	Arenz et al. [5]
4UY8	TnaC	3.8 Å	Bischoff et al. [12]
3JBU	SecM	3.6 Å	Zhang et al. [62]
3JBV	SecM	3.3 Å	Zhang et al. [62]
5NWY	VemP	2.9 Å	Su et al. [54]
5AFI	Empty	2.9 Å	Fischer et al. [17]
5MDZ	Empty	3.1 Å	James et al. [28]
5UYK	Empty	3.9 Å	Loveland et al. [33]
5UYL	Empty	3.6 Å	Loveland et al. [33]
5UYM	Empty	3.2 Å	Loveland et al. [33]
5UYN	Empty	4.0 Å	Loveland et al. [33]
5UYP	Empty	3.9 Å	Loveland et al. [33]
5UYQ	Empty	3.8 Å	Loveland et al. [33]
4YBB	Empty	2.1 Å	Noeske et al.[44]

Table 2.1: List of the structures used to determine the atoms of the ribosomal exit tunnel. All structure, with the exception of 4YBB, were obtained by cryo-EM. 4YBB was obtained using X-ray crystallography.

and residue A94 of 23S are located close to the exit of the tunnel. They defined the center of mass of the exit (COM exit). To reduce the influence of atoms close to the surface of the ribosome, the cylindrical volume ends prematurely on a level with the loop of uL23 (magenta).

Atoms with a SASA $> 9\,\text{Å}^2$ were selected as surface atoms. This threshold is based on the SASA of amino acids [32]. All residues within a distance of 3 Å to surface atoms were chosen as tunnel residues.

Repeating this calculation for all 16 experimental structures resulted in 16 ribosomal exit tunnel. Atoms that were represented in the union of all exit tunnel but not in every structure, were rejected from the selection. Therefore all tunnels contain the same atoms.

The SASA of the tunnel atoms was calculated using the program HOLLOW [23]. A schematic representation of the algorithm is shown in Figure 2.2. HOLLOW

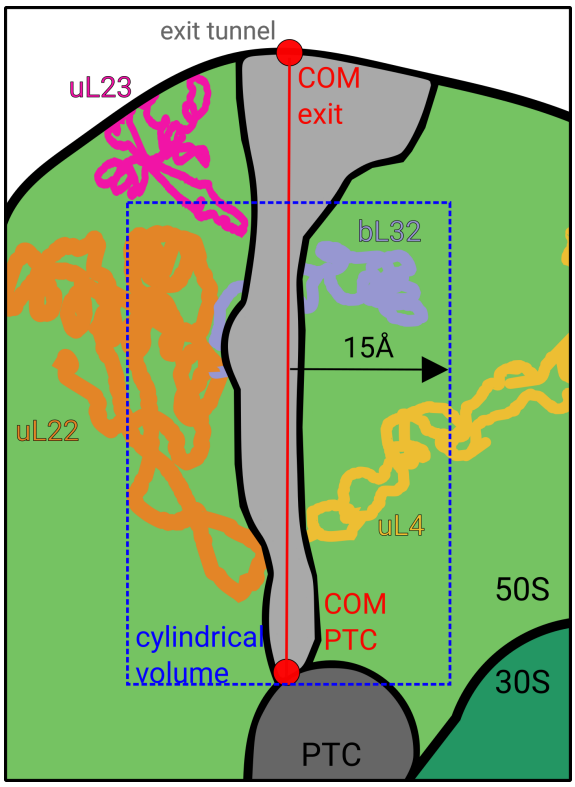

Figure 2.1: Schematic representation of the steps used to define the ribosomal exit tunnel. A selected region of the ribosome is shown. The large subunit (50S, light green) and the small subunit (30S, dark green) together with the proteins uL4 (yellow), uL22 (orange), uL23 (magenta), and bL32 (grey-blue) are shown. The SASA of the atoms was calculated within the cylindrical volume (blue dashed line). The axis of the cylindrical volume is described by the axis of the exit tunnel (red line).

generates a fine spaced grid of probe atoms (blue). No probe atoms overlap with atoms of the structure (grey). To achieve an accurate surface calculation (black line), the grid spacing was set to $d = 0.5\,\text{Å}$. The radius of the dummy atoms was set to $r = 1.4\,\text{Å}$, which corresponds to the van der Waals radius of water molecules [18]. To accelerate the calculations, a pre-selected region of the ribosome was used.

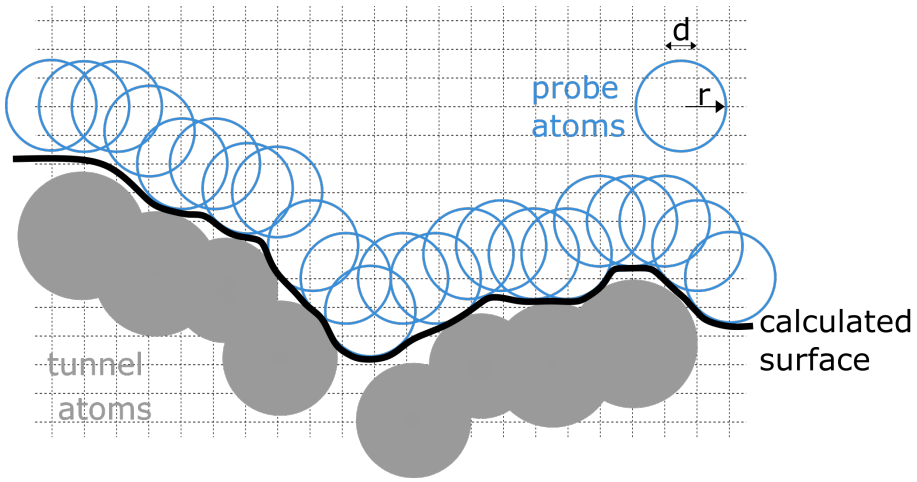

Figure 2.2: Schematic representation of the surface calculation via HOLLOW. Probe atoms (blue) with the radius r get placed on a grid with a grid spacing constant d. The calculated surface of the tunnel atoms (grey) is represented by a black line.

2.2 Backbone definition

To keep an equal number of backbone atoms per residue for proteins and rRNA, the following atoms were selected as backbone atoms. The atoms P, O_3', O_5' and C_3' were selected as rRNA backbone atoms. The backbone of the proteins consists of C, O, N and C_α atoms.

2.3 Molecular dynamics simulation

Contemporary experimental methods, such as cryo-EM or X-ray crystallography, only represent the dynamics of the ribosome to a certain extent. Different conformations of the structure or the temperature factor, also known as B-factor [55], give an estimate about the dynamics. Yet, they are influenced by the intrinsic heterogeneity of the data sets, fitting methods or the instrumental conditions [48]. In addition, the methods require that the ribosome either has to be cooled down to approximately 90 K or has to be arranged in a crystal structure. The resulting

structures are therefore not obtained under physiological conditions.

To analyze the dynamics of the ribosome under physiological conditions, all-atom MD simulations were used in this study. MD simulations are based on the integration of Newton's equations of motion for every particle. The potential that defines the force acting between particles is derived semi-empirically. It results from simplifying the Schrödinger equation with parameters adjusted to experimental observations.

This approach makes it possible to reproduce and predict physical quantities and the behaviour of real systems [53] under the following assumptions.

The time-dependant Schrödinger equation describes a system of N particles at time t

$$i\hbar\frac{\partial}{\partial t}\psi(\boldsymbol{x}_\mathrm{e},\boldsymbol{x},t)=\hat{\mathcal{H}}\,\psi(\boldsymbol{x}_\mathrm{e},\boldsymbol{x},t)\ , \tag{2.1}$$

where ψ denotes the wave function of the system, $\boldsymbol{x}_\mathrm{e}=\left\{\boldsymbol{x}_{\mathrm{e}j}\right\}$ the positions of the electrons and $\boldsymbol{x}=\{\boldsymbol{x}_i\}$ the positions of the nuclei. Currently, it is impossible to solve this equation for sufficiently large systems, such as biomolecules. To simplify the Schrödinger equation, the Born-Oppenheimer approximation was used. Because nuclei are much heavier than electrons, it is assumed that the motion of electrons follows the motion of nuclei instantaneously. Therefore, the motion of the nuclei was separated from the motion of the electrons.

The wave function of the electrons ψ_e given the position of the nuclei is described by

$$\hat{\mathcal{H}}_\mathrm{e}\,\psi_\mathrm{e}(\boldsymbol{x}_\mathrm{e}|\boldsymbol{x})=E_\mathrm{e}(\boldsymbol{x})\ \psi_\mathrm{e}(\boldsymbol{x}_\mathrm{e}|\boldsymbol{x})\ . \tag{2.2}$$

The energy E_e depends on the positions of the nuclei $\boldsymbol{x}$. The equation is time independent.

Under the assumption that the electrons are in a low-energy state, the motion of

the nuclei was approximated by classical Newtonian mechanics

$$m_i \frac{\mathrm{d}^2}{\mathrm{d}t^2} \boldsymbol{x}_i = -\nabla_i E_\mathrm{e}(\boldsymbol{x}_i) \ , \tag{2.3}$$

with m_i being the mass of the i-th particle. The force results from the influence of the electrons on the nucleic motion.

Furthermore, the potential E_e is approximated by an effective potential E_ff, also known as force field [25]

$$E_\mathrm{e} \approx E_\mathrm{ff} = \sum_{\text{bonds}} E_k^{\text{bond}} + \sum_{\text{angles}} E_l^{\text{angle}} \sum_{\text{dihedral}} E_m^{\text{dihedral}} + \sum_{\text{pairs}} \left(E_{ij}^{\text{Coulomb}} + E_{ij}^{\text{vdW}} \right) + \dots \ . \tag{2.4}$$

The interactions between particles are divided into two categories, the bonded and non-bonded interactions. The bonded interactions include terms that approximate for example bond, angle, and dihedral interactions. The non-bonded interactions include van der Waals (vdW) and Coulomb interactions, as shown in equation (2.4).

The parameters describing the force field are either results of *ab initio* calculations or are fine tuned in order to reproduce specific physical quantities.

Currently, large-scale computer clusters, like HYDRA[2] or SuperMUC[3], are able to produce simulation trajectories of macromolecules, such as the ribosome, up to the order of microseconds. Yet biomolecules exhibit motions in a large range of length and time scales. The motions are ranging from femtosecond bond and angle vibrations of sub-angstrom length to large collective motions on a time scale of seconds to minutes. The latter are currently inaccessible through unbiased MD.

The predictive power of MD simulations relies on adequate sampling of the high dimensional conformational space of the macromolecule. Convergence tests were used to give insight about the sampling. While thermal convergence (e.g. pressure,

[2]Max Planck Computing and Data Facility, Garching, Germany
[3]Leibniz Supercomputing Centre, Garching, Germany

density and total energy) was reached fast, other convergence tests were carried out to address biological questions.

2.4 Root mean square deviation

One method to check whether the system has converged, the root mean square deviation (RMSD) from the starting structure was calculated over time. A converged system has sampled all configurations which is represented by a plateau of the RMSD. Before calculating the RMSD, each frame of the trajectories was superimposed to a reference using the least-squares method.

The RMSD is defined as

$$\mathrm{RMSD}(t) = \sqrt{\frac{1}{N_{\mathrm{atoms}}} \sum_{i=1}^{N_{\mathrm{atoms}}} \Big(\boldsymbol{x}_i(t) - \boldsymbol{x}_i(t_0)\Big)^2}, \tag{2.5}$$

where N_{atoms} is the number of atoms, $\boldsymbol{x}_i(t)$ is the i-th atom coordinate of the structure at time t.

2.5 Principal component analysis

Possible large-scale collective slow motions of the ribosomal exit tunnel may be obscured by fast small-amplitude thermal vibrations. To extract these large-scale collective slow motions, a principal component analysis (PCA) [4] was applied on the trajectories.

The PCA is based on the covariance matrix $\boldsymbol{C}$. The entries of the the covariance matrix were constructed from the Cartesian coordinates of the tunnel atoms of the trajectories. Assuming that the motion of heavier atoms contributes more to large scale motions, the entries were mass-weighted. In addition, to make the result

comparable to Cartesian units, each entry was divided by $\sqrt{3N}$ [1].

The entries of the covariance matrix are then defined as

$$C_{ij} := \Big\langle \left(x_i - \langle x_i \rangle\right)^{\intercal} \left(x_j - \langle x_j \rangle\right) \Big\rangle , \tag{2.6}$$

where $x_1, \ldots, x_{3N}$ are the mass-weighted and by $\sqrt{3N}$ divided Cartesian coordinates of the N tunnel atoms, and $\langle \ldots \rangle$ denotes the time average.

The covariance matrix $\boldsymbol{C}$ of the data set was diagonalized. The eigenvectors of the covariance matrix $\boldsymbol{C}$ were sorted according to their eigenvalues. The first eigenvector has the largest eigenvalue, the last eigenvector has the smallest. The projection of the trajectory on the first eigenvector is called first principal component (PC 1). It reveals the motion with the largest variance of the system. The projection on the second eigenvector is called second principal component (PC 2), and so on. Principal components are also referred to as modes.

The contribution Λ_i of the i-th principal component λ_i to the total motion was calculated

$$\Lambda_i = \frac{\lambda_i}{\sum_n \lambda_n} , \tag{2.7}$$

with the summation over all principal components. The contributions are also referred to as the spectrum of the eigenvalues.

Principal components of high dimensional diffusion are cosines. The resemblance of a principal component q_i with a cosine is called cosine content c_i [21]. Analysis of principal components with regard to their cosine content was used to further assess the convergence of the trajectories.

The cosine content c_i of the i principal component is defined as

$$c_i = \frac{2}{T} \left(\int_0^T \cos\!\left(\frac{i\pi t}{T}\right) q_i(t)\, \mathrm{d}t \right)^2 \left(\int_0^T q_i^2(t)\, \mathrm{d}t \right)^{-1} , \tag{2.8}$$

where T is the length of the analyzed trajectory.

2.6 Trajectories of different length & nomenclature

The trajectories analyzed in the present study differ in their length. Restricting all trajectories to the smallest sampled time period is a waste of information. To make the trajectories comparable without losing information from long trajectories, all trajectories were assigned the same statistical weight.

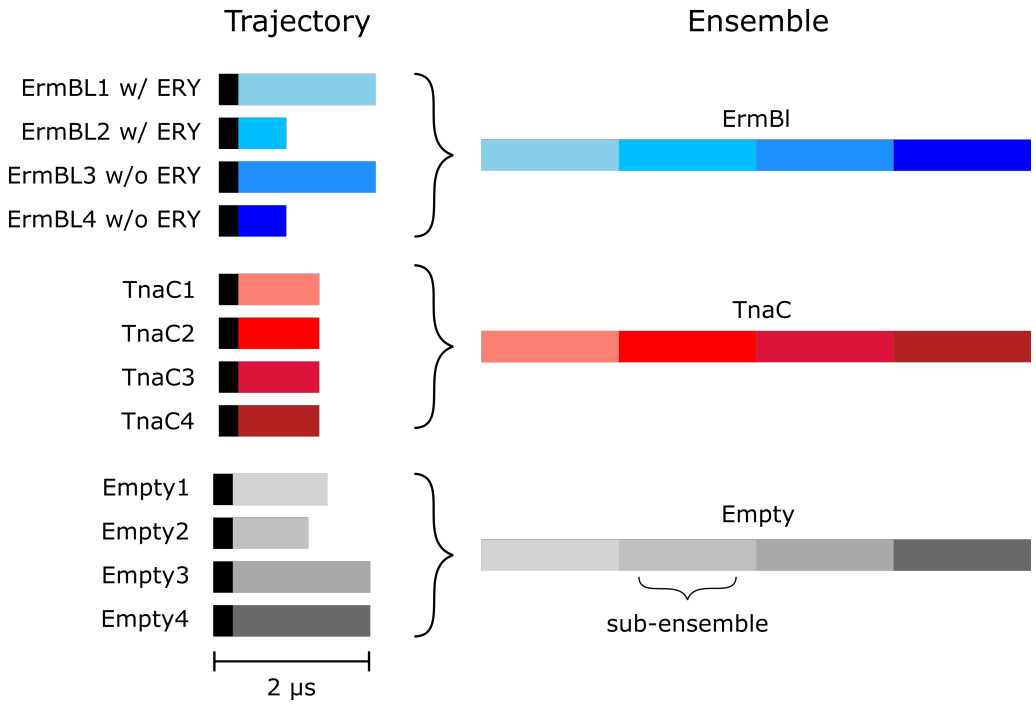

Figure 2.3: Illustration of the length of the analyzed trajectories. The trajectories are colored according to the system they represent: ribosome with ErmBL (shades of blue), ribosome with TnaC (shades of red) and the empty ribosome (shades of grey). A fixed part of each trajectory was omitted (black) before constructing the sub-ensembles. All trajectories were assigned the same statistical weight, as illustrated in the length of the sub-ensembles.

Figure 2.3 illustrates this approach and introduces the following nomenclature. The trajectories analyzed in this thesis are named after the system they represent and were consecutively numbered. In the case of the ErmBL trajectories, the pres-

ence (w/ ERY) or absence of the antibiotic erythromycin (w/o ERY) is indicated as well. After all trajectories were assigned the same statistical weight, they are referred to as sub-ensembles. The unions of the four sub-ensembles of each system are referred to as ensembles. The union of all ensembles is called supra-ensemble. This nomenclature will be applied throughout the thesis. The details of the simulations will be addressed in chapter 3.

2.7 Root mean square fluctuation

To detect mobile regions of the ribosomal exit tunnel, the root mean square fluctuation (RMSF) of its constituents was calculated. Before calculating the RMSF, each frame of a trajectory was superimposed to a reference using the least-squares method.

To estimate an error, the RMSF of the i-th particle was calculated for each sub-ensemble

$$\mathrm{RMSF}_i^{\text{sub-ensemble}} = \sqrt{\frac{1}{N_{\text{conf.}}} \sum_{n=1}^{N_{\text{conf.}}} \left(\boldsymbol{x}_i(n) - \langle \boldsymbol{x}_i \rangle_{\text{ensemble}} \right)^2}, \tag{2.9}$$

where $N_{\text{conf.}}$ is the number of conformations of the sub-ensemble. The average position of the i-th atom was calculated over the ensemble which consists of four corresponding sub-ensembles

$$\langle \boldsymbol{x}_i \rangle_{\text{ensemble}} = \frac{1}{4 \cdot N_{\text{conf.}}} \sum_{n=1}^{4 \cdot N_{\text{conf.}}} \boldsymbol{x}_i(n) \ .$$

For each ensemble, the RMSF of the sub-ensembles were averaged. Resulting in a RMSF of each particle for each ensemble. The corresponding standard error was used to estimate the error of the calculation.

3 MD Simulation Protocols

The analyzed trajectories of the ribosome with and without peptides were kindly provided by Lars V. Bock [1] and Michal H. Kolář [1]. Here, I briefly summarize how the trajectories were originally obtained.

First, I will present the general setup that is common for all simulations in this thesis. The computational details that are specific for individual simulations are described further below.

3.1 General simulation setup

The general approach of the simulation setup is the following.

All simulations started from experimentally determined structures. The structures were solvated in water under physiological conditions regarding the temperature, pressure and salinity. The starting structure might be in a conformation where very high forces are acting on its atoms. Furthermore, the system was altered by adding the solvent, ions or even changing the solute itself. Starting a simulation directly from this configuration would cause the system to blow up. Therefore the potential energy of the system was minimized in the next step. The positions of the solute were restrained. Thermostats and barostats were used to set and maintain a constant temperature and pressure of the system. During that period ions had time

[1]Max Planck Institute for Biophysical Chemistry, Am Faßberg 11, 37077, Göttingen, Germany.

to rearrange and neutralize highly charged parts of the solute. After the solvent was equilibrated into a a local free energy minimum, the restraints were gradually released. The production run was started without any restraints, allowing the solute to adapt new conformations.

The total length of the trajectories analyzed in this thesis was 17.5 µs, following the detailed simulation protocol as listed below.

3.2 Detailed simulation setup

All MD simulations were carried out using GROMACS 5 [50] with the amber99sb force field [25] or amberff10 force field [49] with refined parameters for nucleic acids [2]. The SPC/E force field [9] was used for water. Force field parameters determined by Joung and Cheatham [29] were used for ions.

For each simulation, the corresponding cryo-EM structure was used as the starting structure. Each structure was solvated with water molecules in a dodecahedron box with periodic boundaries. A minimum distance of 1.5 nm was kept between the non-solvent atoms and the box boundaries.

The systems were neutralized with K^+ ions and both $MgCl_2$ and KCl salt were added using GENION, a program of the GROMACS simulation package. [50]. The ion and salt concentrations were chosen to reproduce the experimental conditions.

Lennard-Jones and short-range electrostatic interactions were calculated within a distance of 1 nm during all computational steps Long-range interactions beyond 1 nm were calculated using particle-mesh Ewald summation [16] with a grid spacing of 0.12 nm. Bond lengths were constrained using the LINCS algorithm [22]. The production runs of the simulations were preceded by the following multi-step equilibration protocols whose details are system specific.

3.2.1 ErmBL

The simulations containing the ErmBL peptide were prepared and carried out by L. V. Bock, H. Grubmüller and A. C. Vaiana. The details regarding the setup of the simulations were adapted from the methods presented by Arenz et al. [6].

The ErmBL simulations were started from the cryo-EM structure of the ribosome in complex with two tRNAs at A and P-site (PDB 5JTE) [6]. Four independent simulations have been carried out. From which two were started from the cryo-EM structure including the antibiotic ERY (ErmBL w/ ERY), and the other two form the cryo-EM structure after ERY was removed (ErmBL w/o ERY).

During the simulations, the temperature was set to 300 K, while the solute and solvent were controlled independently via velocity rescaling [13] with a coupling constant of $\tau_T = 0.1\,\mathrm{ps}$. The integration time step was set to 4 fs.

The equilibration of the system was carried out in three steps:

1. Energy minimization via steepest descent algorithm.

2. 0 ns to 50 ns: Applying Berendsen barostat [10] ($\tau_p = 1\,\mathrm{ps}$) and restraining positions of all heavy atoms that are included in the cryo-EM structure with restraining force constant $k = 1000\,\mathrm{kJ\,mol^{-1}\,nm^{-2}}$, heavily penalizing a deviation from the initial conditions.

3. 50 ns to 70 ns: Linear decrease of position restraint force k to zero.

The production was run from 70 ns to 2070 ns, while applying the Parrinello-Rahman barostat [47] with a coupling constant $\tau_p = 1\,\mathrm{ps}$ and no position restraints. While the trajectories ErmBL1 w/ ERY and ErmBL3 w/o ERY had a length of 2 µs, the trajectories ErmBL2 w/ ERY and ErmBL4 w/o ERY had a length of 0.86 µs due to a shorter production run.

3.2.2 TnaC

The simulations containing the TnaC peptide were prepared and carried out by Michal H. Kolář. The starting conformation of the ribosome was adapted from coordinates observed by cryo-EM (PDB 5AFI [17]). The TnaC peptide, taken from PDB 4UY8 [12], was then fitted into the empty structure. This process allowed to benefit from the high resolution of the structure of the empty ribosome (PDB 5AFI).

Tryptophan, which is necessary for stalling to occur, was not present in the simulations to enhance the conformational flexibility of the nascent chain inside the ribosomal exit tunnel.

The equilibration of the system was carried out in six steps:

1. While applying positional restraints with force constant $k = 5000\,\mathrm{kJ\,mol^{-1}\,nm^{-2}}$ on the backbone atoms of the system, the energy was minimized via steepest descent algorithm.

2. 0 ns to 1.5 ns: Assigning initial velocities at a temperature of 10 K for all atoms. The temperature of the solvent (310 K) and the solute (10 K) were controlled via velocity rescaling [13] with a coupling constant of $\tau_T = 0.5\,\mathrm{ps}$. The integration time step was set to 2 fs.

3. 1.5 ns to 21.5 ns: While keeping the position restraints on the backbone atoms, the Berendsen barostat was applied with a pressure of 1 bar and a coupling constant of $\tau_p = 1\,\mathrm{ps}$. The temperature coupling was set to $\tau_T = 1\,\mathrm{ps}$.

4. 21.5 ns to 46.5 ns: Linear increase of the solute thermostat from 10 K to 310 K in 20 ns and further equilibration for 5 ns.

5. 46.5 ns to 66.5 ns: The integration time step was set to 1 fs. Linear decrease

of the restraining force constant k to $0\,\mathrm{kJ\,mol^{-1}\,nm^{-2}}$. The temperature and pressure coupling constants were set to $\tau_p = \tau_T = 2\,\mathrm{ps}$.

6. 66.5 ns to 118.5 ns: First, the temperature the whole system controlled via single velocity rescaling thermostat and the time step was set to $\tau_T = 2\,\mathrm{fs}$, for 21 ns . Then for additional 31 ns, the Parrinello-Rahman barostat [47] with a coupling constant $\tau_p = 2\,\mathrm{ps}$ was applied.

Beginning from step 6, four independent trajectories were generated by random velocity assignment. This resulted in four production runs at a temperature of 310 K, with the integration time step set to 4 fs. The calculated trajectories had a length of 1.28 µs.

3.2.3 Empty

Two of the empty ribosome simulations were provided by Michal H. Kolář (Empty1 and Empty2) and the other two by Lars V. Bock (Empty3 and Empty4). The starting conformation of all four simulations was based on the cryo-EM structure of an empty ribosome (PDB 5AFI [17]).

The equilibration protocol of Empty3 and Empty4 simulations was identical with the equilibration protocol of the ErmBL simulations (section 3.2.1). Both trajectories were 2.0 µs long.

The equilibration of the simulations Empty1 and Empty2 was done in four steps:

1. While applying positional restraints with a force constant $k = 1000\,\mathrm{kJ\,mol^{-1}\,nm^{-2}}$ on the backbone atoms of the system, the energy was minimized via steepest descent algorithm.

2. 0 ns to 1 ns: Assigning initial velocities at 10 K for all atoms. The temperature of the solvent (310 K) and the solute (10 K) were controlled via velocity

rescaling [13] with a coupling constant of $\tau_T = 0.5\,\mathrm{ps}$. The integration time step was set to 1 fs.

3. 1 ns to 10 ns: While keeping the position restraints on the backbone atoms, the Berendsen barostat was applied with a pressure of 1 bar and a coupling constant of $\tau_p = 1\,\mathrm{ps}$. The temperature coupling constant was set to $\tau_T = 1\,\mathrm{ps}$. The integration time step was set to 2 fs.

4. 10 ns to 50 ns: The integration time step was set to 4 fs. Linear decrease of the restraining force constant to $k = 0\,\mathrm{kJ\,mol^{-1}\,nm^{-2}}$ while the temperature was set to 310 K. The temperature and pressure coupling constants were set to $\tau_p = \tau_T = 2\,\mathrm{ps}$.

The production was run while applying the Parrinello-Rahman barostat [47] with a coupling constant $\tau_p = 2\,\mathrm{ps}$ and with an integration time step of 4 ps. Beginning from step 2, two independent trajectories were generated by random velocity assignment. Empty1 had a length of 1.45 µs. Empty2 had a length of 1.2 µs. While Empty1 and Empty2 were run at a temperature of 310 K, Empty3 and Empty4 were run at a temperature of 300 K.

4 Results and Discussion

Here, I will address two main questions. First, what are the dynamics of the ribosomal exit tunnel. Second, how are these dynamics affected by the nascent chain.

4.1 Structure of the ribosomal exit tunnel

By applying the definition of the ribosomal exit tunnel (section 2.1), 16 exit tunnel structures were obtained. All tunnels contain the same atoms by construction. Figure 4.1 shows the structure of the ribosomal exit tunnel, based on the high resolution crystal structure of an empty ribosome (PDB 4YBB).

The ribosomal exit tunnel walls contain 3855 atoms which belong to 219 residues. The tunnel wall is largely made up by rRNA (grey) with 153 residues. Additionally, the four proteins uL4 (yellow), uL22(orange), uL23 (magenta), and bL34 (not shown), are part of the ribosomal exit tunnel walls with 66 residues .

To quantify the structural differences between the high resolution empty tunnel (PDB 4YBB) and the remaining 15 tunnels, the RMSD was calculated (Fig. 4.2). Before the calculations, the structures were superimposed with the backbone atoms of the empty exit tunnel (PDB 4YBB). The all-atom RMSD (plain) and the backbone RMSD (hatched) were calculated.

The all-atom RMSD (plain) ranges between 0.78 Å and 1.16 Å. Tunnels containing a peptide (bright colors) adopt similar RMSD values as tunnels without one (grey).

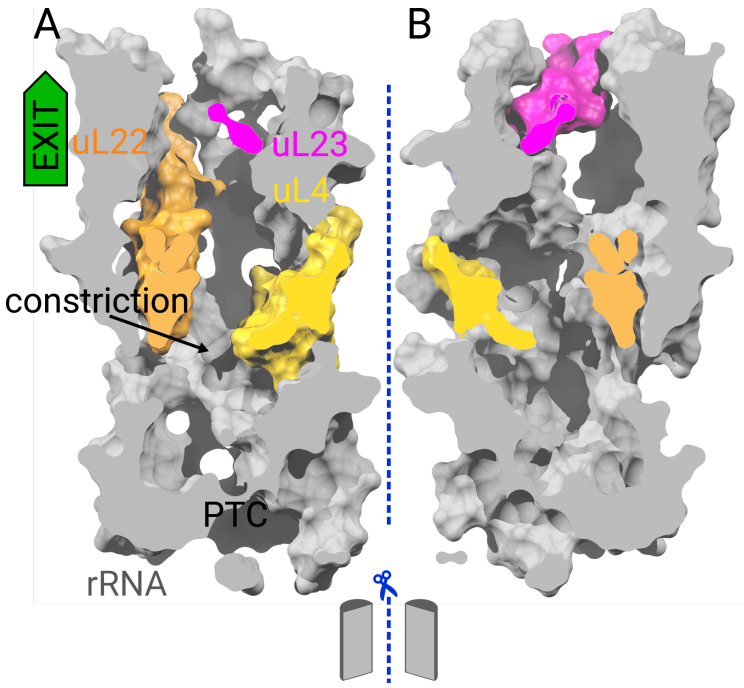

Figure 4.1: Structure of an empty exit tunnel (PDB 4YBB). The tunnel was clipped a plane parallel to the tunnel axis. Both halves (A and B) are shown. Ribosomal RNA is depicted in grey; ribosomal proteins uL4 in yellow, uL22 in orange, and uL23 in magenta. Protein bL34 is not visible in this representation although part of the exit tunnel.

The RMSD values suggest that the peptide inside the tunnel does not majorly influence the static structure of the ribosomal exit tunnel.

The backbone RMSD (hatched) follows the trend of the all-atom RMSD, albeit with lower values. The lower backbone RMSD indicate that the conformation of the backbone is more preserved throughout the tunnels, compared to the conformation of all atoms.

The exit tunnels with ErmBL present (blue) are more similar to the empty reference tunnel (PDB 4YBB) than other empty exit tunnel (grey). This similarity suggests that the global structure of the tunnel is not influenced by the presence of a peptide. However, small structural changes resulting from interactions of single side chains with the peptide cannot be detected by the RMSD. Yet it was shown that small conformational changes of single nucleotides are caused by the nascent

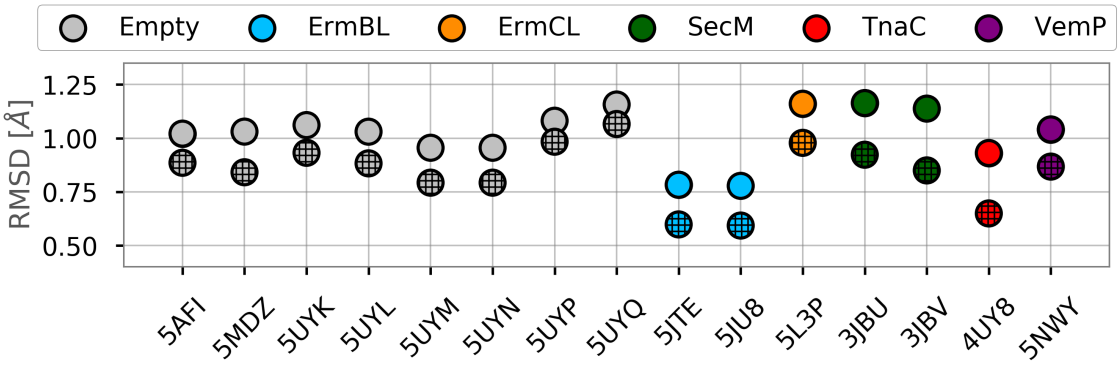

Figure 4.2: All-atom RMSD (plain) and backbone RMSD (hatched) to the reference tunnel structure for the remaining 15 exit tunnel as extracted from experimental structures. The color code shows what kind of peptide was present inside the ribosomal exit tunnel.

chain and contribute to translational stalling [6].

Furthermore, the RMSD questions the effect of models and refinement used for fitting cryo-EM densities. Generally, cryo-EM structures are not obtained *de novo*. Rather, structures are based on knowledge provided by X-ray crystallography. The observed similarities might well be caused by the way the structures where obtained from the data. Particularly, the ErmBL structures (PDB 5JTE, PDB 5JU8) were modeled based on a X-ray structure (PDB 4U26 [43]) from Noeske et al. from the Cate Lab[1], which also provided the high resolution reference structure (PDB 4YBB [44]) the RMSD was calculated from.

Therefore we asked, what are the dynamics of the ribosomal exit tunnel?

4.2 Convergence of the simulations - Part I

To estimate the robustness of the conclusions that can be drawn from the simulations, the convergence of the simulations was assessed.

The trajectories were superimposed by least-square fitting to the high resolution

[1]Department of Molecular and Cell Biology, University of California, Berkeley, California, USA

empty tunnel (PDB 4YBB) based on protein and rRNA backbone atoms. All-atom RMSD, protein backbone RMSD and rRNA backbone RMSD were calculated according to equation (2.5), as described in chapter 2.

Figure 4.3 (left column) shows the all-atom RMSD. After 0.25 µs simulation time, ErmBL (shades of blue) and Empty (shades of grey) yield an all-atom RMSD of about 0.22 nm. Whereas TnaC (shades of red) yields an all-atom RMSD of about 0.16 nm. These values are approximately constant throughout the remaining simulation.

However, the RMSD curves of the trajectories ErmBL1 w/ ERY, ErmBL2 w/ ERY, ErmBL3 w/o ERY, Empty1, and Empty3 show small tendencies of a drift towards higher RMSD values. The curve of TnaC2 indicates that a further increase of RMSD values is likely if simulations were continued. The all-atom RMSD indicates that the simulations have converged into a local minimum.

The lower RMSD values of TnaC trajectories could be explained by the presence of the long TnaC peptide. Due to presence of the peptide a conformation closer to the starting conformation might be energetically preferred. To test that hypothesis, the peptide could be removed from the ribosome during the simulation.

Figure 4.3 (right column) shows the backbone RMSD for proteins (black) and rRNA (dark green). The protein backbone RMSD yields higher values than the all-atom RMSD. In addition, drifts (ErmBL1 w/ ERY) and multiple jumps (TnaC1, TnaC2, TnaC4, Empty1, Empty2, Empty3, and Empty4) are present. The rRNA backbone RMSD yields lower values than the all-atom RMSD. A plateau of about 0.16 nm is quickly reached. Only small deviations from this value are present.

Jumps in the protein backbone RMSD indicate transitions between multiple conformations and suggest that the proteins are more flexible and explore the conformation space on a faster time scale than rRNA does. The lower rRNA backbone

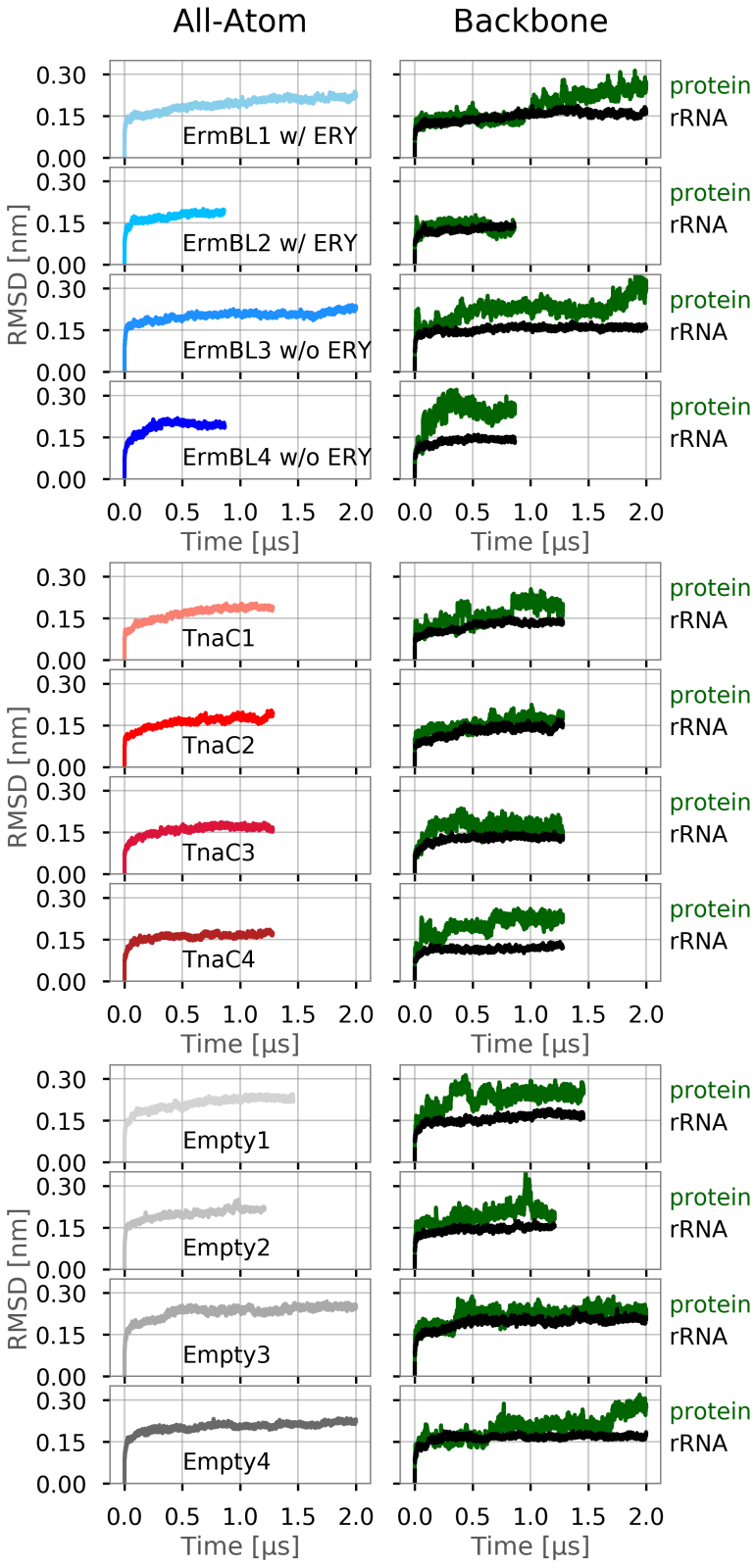

Figure 4.3: RMSD calculations of the ribosomal exit tunnel. Left column shows the all-atom RMSD. The curves are colored according to the peptide present. Right column shows protein backbone RMSD (black) and rRNA backbone RMSD (dark green).

RMSD values indicate that the rRNA is the more rigid part of the ribosomal exit tunnel.

As presented in chapter 3, the simulations were run at different temperatures. To assess the influence of the temperature, the RMSD of the Empty simulations were compared. Empty1 and Empty2 were simulated at 310 K, Empty3 and Empty4 at 300 K, yet the RMSD yields similar values regardless of the temperature. Hence, it suggests that a temperature difference of 10 K does not influence the dynamics of the exit tunnel.

While reaching a plateau of the RMSD is a necessary condition for convergence, it is not a proof. The RMSD curves indicate that a local minimum was reached. But there are also regions of the phase space that were not sampled. Further convergence test were therefore necessary to estimate the sampling.

4.3 Convergence of the simulations - Part II

To further assess the convergence of the simulations, the cosine content of the principal components of the individual trajectories was calculated according to equation (2.8), section 2.5.

Figure 4.4 shows the cosine content c_i of the trajectories. The corresponding covariance matrices were constructed from each trajectory. For most trajectories, the cosine content yields a value close to 1 for the first principal component. Only trajectories ErmBL3 w/o ERY and ErmBL4 w/o ERY yield lower cosine content values around 0.6 for the first principal component. The cosine content decays non monotonically towards lower values with increasing principal component index.

The generally high cosine content of the first three principal components suggest that the motion of the exit tunnel along these eigenvectors resembles an unbiased diffusive motion. The cosine content contradicts the assumption that the simulations

are converged in a local minimum. It rather suggests a constant, flat free energy potential. However, combining the information provided by all trajectories might give a first estimate about the global free energy landscape.

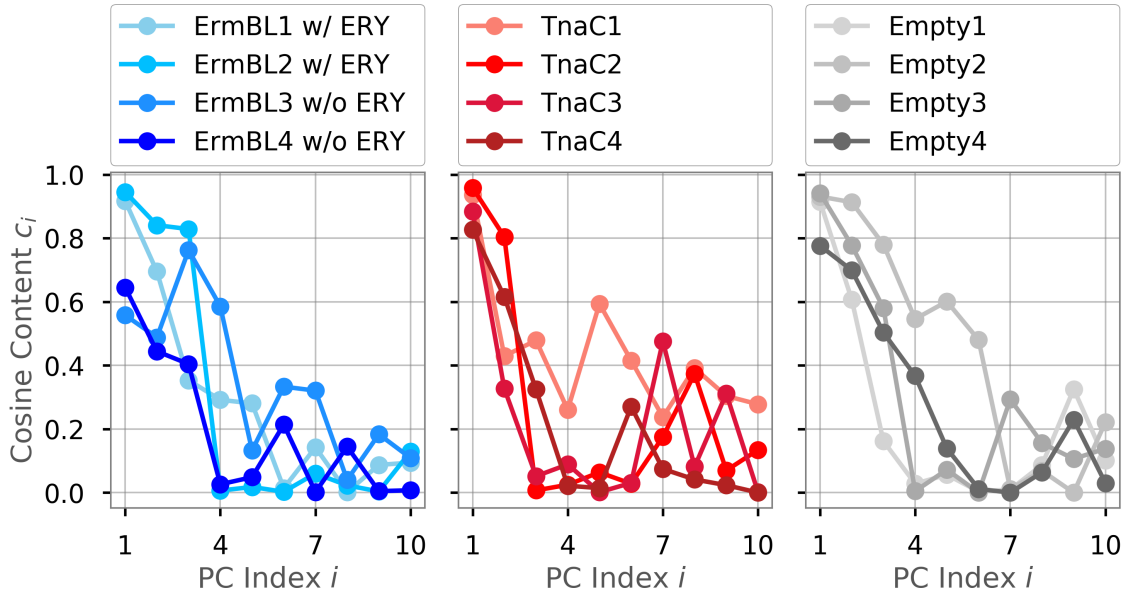

Figure 4.4: The cosine content c_i of the first ten principal components (PC) is shown. The colors indicate the individual trajectories.

4.4 Conformational dynamics of the exit tunnel

As explained in section 2.5, PCA was used to detect the large-scale, collective slow motions of the ribosomal exit tunnel. Here we address the following questions. What are the conformational motions of the exit tunnel? And are conformational motions affected by nascent chains?

The covariance matrix was constructed from the supra-ensemble. As defined in section 2.6, the supra-ensemble is the union of the three ensembles ErmBL, TnaC and Empty.

To reduce the influence of the equilibration process, the first 0.25 µs of each trajectory were omitted, when constructing the ensembles. This value was suggested

by the RMSD calculations (Fig. 4.3).

The spectrum was calculated according to equation (2.7), section 2.5. Both the eigenvalue spectra and the principal components varied only slightly when the first 0.1 µs to 0.5 µs of each trajectory were omitted. This suggests that the result is not sensitive to the length of the omitted trajectory.

As shown in Figure 4.5, the first principal component contributes with 13.3 % and the first three principal components together with 30 % to the total motion of the ribosomal exit tunnel. The contribution of each other principal component is less than 7.3 %. The spectrum indicates that the ribosomal exit tunnel does not undergo one large-scale motion but rather many smaller ones.

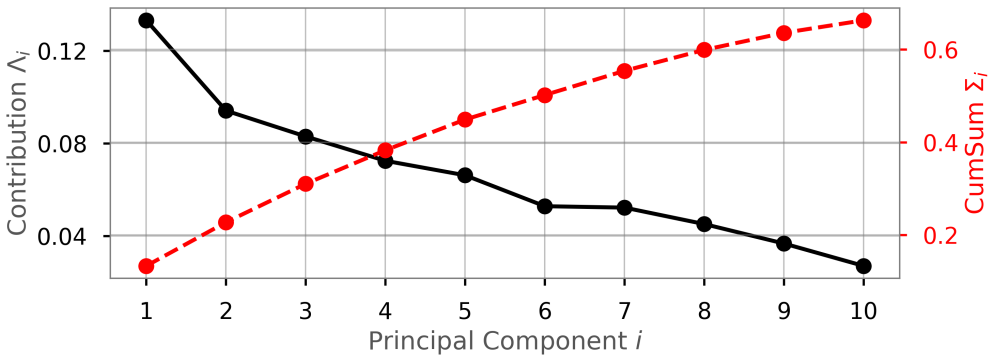

Figure 4.5: Spectrum of the eigenvectors (black) and the cumulative sum (Cum Sum) up to the i-th principal component (red). Shown are the first ten principal components. In order to calculate the contribution of each principal component to the total motion, each eigenvalue gets normalized by the sum over all eigenvalues.

The projection of all analyzed trajectories on the first three eigenvectors is shown in Figure 4.6. The trajectories of the three systems ErmBL, TnaC and Empty cluster in these projections, while partially overlapping with each other. The projections indicate that no individual mode is able to distinguish between the conformations of the exit tunnel with respect to the peptide

Yet, the trajectories partially separate from the starting structures that are clus-

tered in the center along all three projections. The partial separation suggests that small differences in the structures cause noticeable differences in the conformational dynamics of the exit tunnel. These conformational differences support that RMSD calculations were not sensitive enough to capture the structural differences.

Firstly, I will focus on the space spanned by the first and the second mode (Fig. 4.6, A). The first and the second mode combined are able to distinguish between the conformations of the tunnel with ErmBL (shades of blue) or TnaC (shades of red) present and the empty tunnel (shades of grey). Yet, the simulations ErmBL4 w/o ERY, TnaC4 and Empty4 partially overlap. The set of TnaC and Empty simulations neither separate along the first mode nor along the second one. Hence, the first and second mode will be used to investigate the differences between the conformations of the exit tunnel with ErmBL and the empty tunnel.

Secondly, the projection on the first versus the third eigenvector (Fig. 4.6, B) shows a partial separation between the conformations of the exit tunnel with a TnaC peptide and an empty one. A projection of a TnaC trajectory (TnaC3) is overlapping with a projection of a trajectory of an empty exit tunnel (Empty1). Less trajectories overlap along the third mode than along the second one. Therefore the first mode and the third mode will be used to investigate the difference in conformational dynamics between the exit tunnel with TnaC and the empty tunnel.

Along all three modes, the projections of Empty trajectories (300 K and 310 K) separate from each other like TnaC (310 K) or ErmBL trajectories (300 K) do. This similarity suggests that the projections along all three modes were not influenced by the temperature difference of the system. This result is supported by RMSD calculations (section 4.2).

The set up of the TnaC simulations might explain the overlap of the projections of TnaC and Empty trajectories. Both Empty and TnaC simulations are based

on an empty ribosome structure (PDB 5AFI). The peptide was modeled into this structure for TnaC simulations. Because of high structural similarity, similar conformations were adapted during the simulation. Furthermore, the projections of individual TnaC trajectories seem to cluster more than the trajectories of the other systems. The presence of the long TnaC peptide seems to restrict conformations of the tunnel. A trajectory that starts from a structure with a resolved TnaC peptide (PDB 4UY8 [12]) might have behaved differently.

To further investigate the differences between the structures obtained by X-ray crystallography and cryo-EM, the projections of the structures along the first three modes are shown in Figure 4.7. The figures show an enlarged version of the region that was marked with the black square in Figure 4.6.

All crystal and cryo-EM structures cluster close to the origin. The structures scatter along all three principal components in the order of 1 Å. No separation can be deduced according to the type of peptide.

The crystal structure of the empty tunnel (PDB 4YBB) and the cryo-EM structures of the tunnel with ErmBL (PDB 5JTE, PDB 5JU8) seem to separate from the other structures along the first mode. This separation supports that the experimental method might influence the conformation of the exit tunnel more than the presence of a nascent chain. Furthermore, the two structures of the tunnel with ErmBL overlap completely. While the one structure (PDB 5JTE) is not in complex with E-site or P-site tRNA, the other one (PDB 5JU8) is. The overlap in the projections suggests that the presence of tRNA does not cause large conformational changes of the exit tunnel. However, small conformational changes, such as those of single side chains, are not represented in the first three modes.

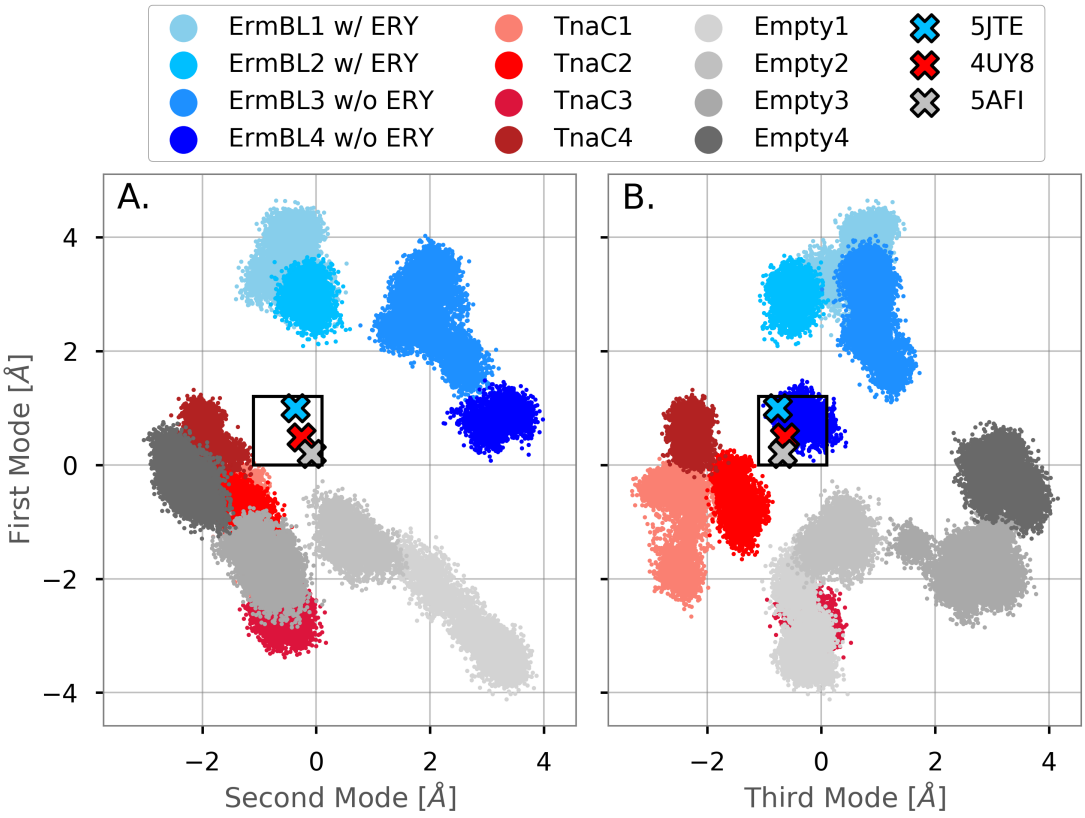

Figure 4.6: Projection of the sets of trajectories onto the first three eigenvectors. The trajectories of the ribosomal exit tunnel with an ErmBL peptide are shown in shades of blue, those with a Tnac peptide in shades of red and those of an empty tunnel in shades of grey. The black square indicates the enlarged area of the projections of the cryo-EM and crystal structures (Figure 4.7). The crosses denote the starting structures of the simulations. The colors indicate the type of peptide.

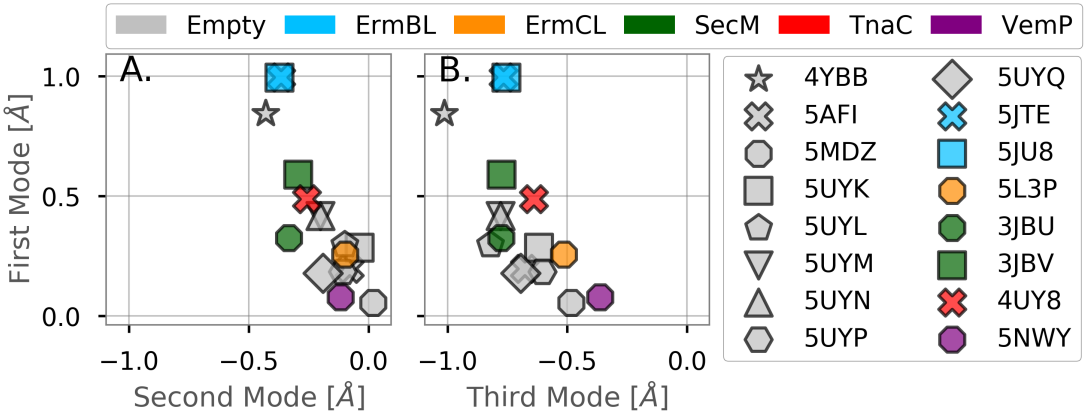

Figure 4.7: Projection of the experimentally obtained structures of the ribosomal exit tunnel. The structures are colored according to the type of peptide present in the tunnel: Empty (grey), ErmBL (lightblue), ErmCL (orange), SecM (green), TnaC (red) or VemP (purple). The crystal structure of the empty tunnel obtained by crystallography (PDB 4YBB) is represented with a star.

To visualize the motion along the eigenvectors, the interpolation between the extreme conformations of the first three modes is shown in Figure 4.8.

As suggested by Figure 4.6, the first and second mode will be used to investigate the conformational differences between the exit tunnel with ErmBL and the empty tunnel. The first and third mode will be used to investigate the conformational differences between the exit tunnel with TnaC and the empty tunnel.

Along all projections, the proteins of the exit tunnel dominate the conformational dynamics. The first and second mode show that protein uL23 adapts conformations pointing towards the exit (up, blue) and away from the exit (down, green) conformation. While proteins of the constriction site (uL4 and uL22) adopt conformations radially closer to the tunnel axis (in, blue) and radially further away (out, green).

The extreme conformations of the third mode are similar to the ones of the first and second mode. In addition, the proteins adapt a slightly twisted conformation.

The extreme conformations of the exit tunnel indicate that the extreme conformations of the ribosomal proteins are influenced by the peptide. The proteins of the exit tunnel seem to prefer an up and in conformation if ErmBL is present (Mode 1 and 2) and an additional slightly twisted conformation if TnaC is present (Mode 3). Yet, as seen in Figure 4.6, these seemingly preferred conformations only represent the extreme conformations of the tunnel. As seen in Figure 4.6, they do not distinguish clearly between the type of the peptide.

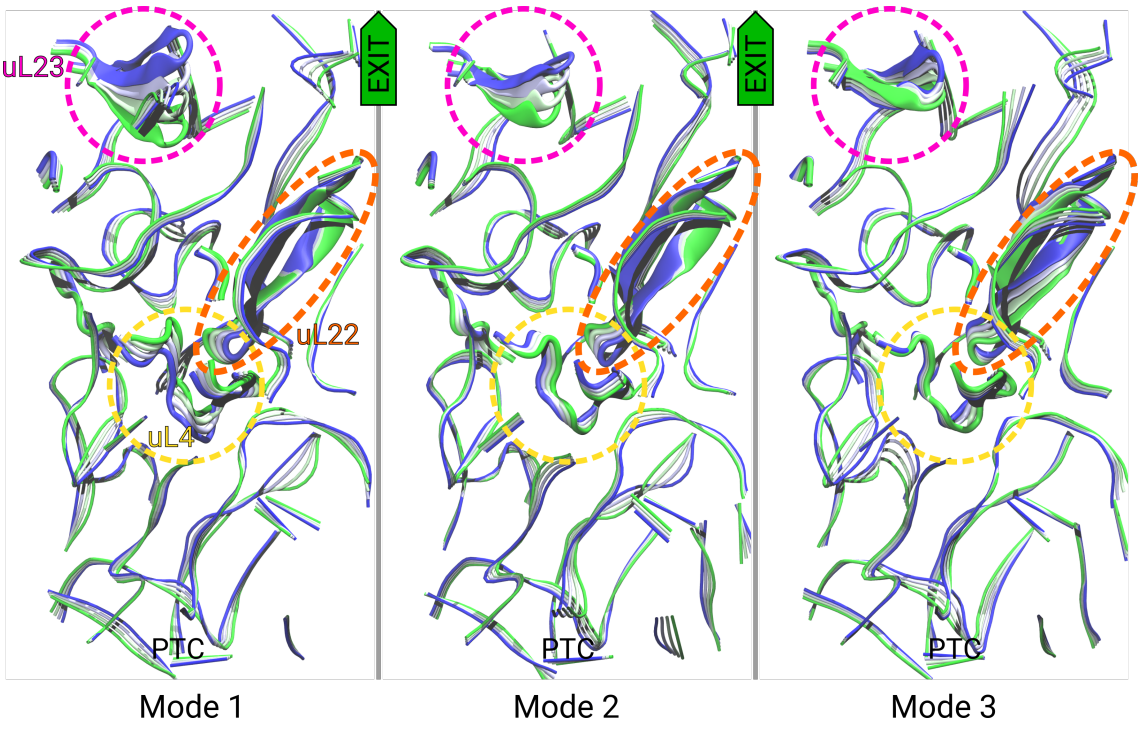

Figure 4.8: Side view of the first (Mode 1), second (Mode 2) and the third mode (Mode 3) of the ribosomal exit tunnel. The interpolated conformations between the two extreme conformations (green and blue) are shown. They were calculated from the projection on the corresponding eigenvectors. While green indicates the extreme conformation of an empty tunnel, blue indicates the conformation with ErmBL (Mode 1 and Mode 2) and TnaC (Mode 1 and Mode 3).

4.5 Flexibility of the exit tunnel

To further assess the difference in dynamics caused by the presence of a peptide, the RMSF of the backbone atoms of the ribosomal exit tunnel was calculated according to equation (2.9), chapter 2. Before calculations, each structure of the ensembles was superimposed with the backbone of the high resolution empty tunnel (PDB 4YBB). Analog to the PCA, the first 0.25 µs of the trajectories were omitted, as suggested by the RMSD (Fig. 4.3).

The result is displayed in two ways. First, the three dimensional structure of the exit tunnel is shown in Figure 4.9. The backbone was colored according to the RMSF values calculated for each ensemble ErmBL, TnaC and Empty. The tunnel

has an average RMSF of approximately 1.2 Å. The three dimensional representation suggests that no orientational dependence of the RMSF exists.

Ribosomal proteins yield higher RMSF values than rRNA for all ensmebles. However, some residues of the rRNA adapt values above the average. The empty exit tunnel has increased values at the three proteins uL4, uL22 and uL23. The exit tunnel with ErmBL or TnaC present has an overall lower RMSF compared to the empty tunnel. Especially protein uL22 seems to be influenced by the presence of a peptide. On the contrary, the RMSF of protein uL23 is unchanged for all three ensembles. Therefore uL23 seems to be unaffected by the presence of the peptide.

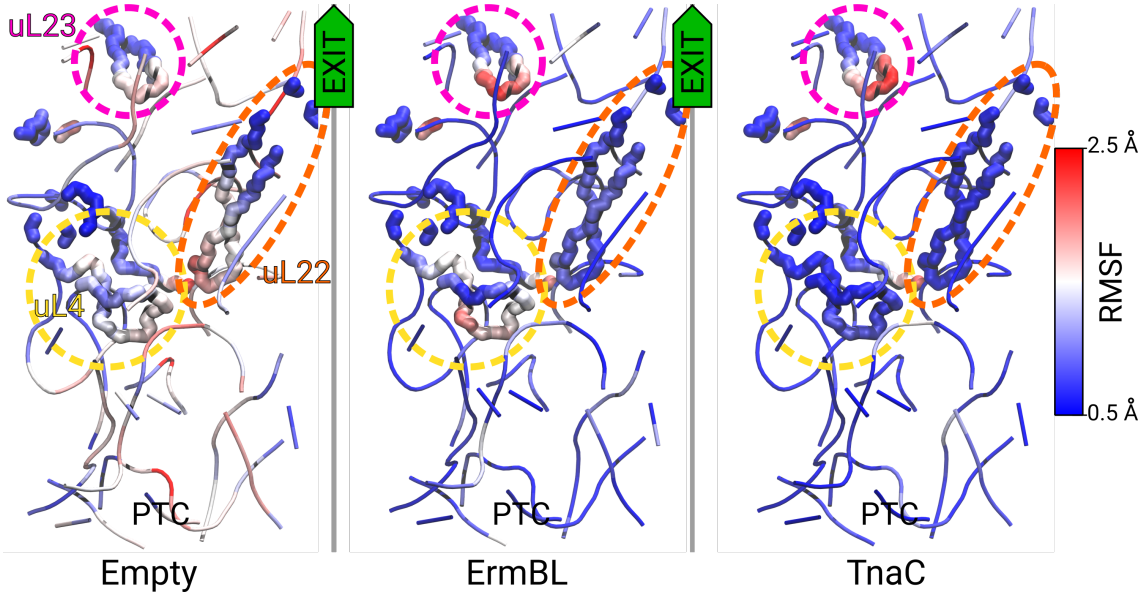

Figure 4.9: Structure of the ribosomal exit tunnel. The backbone was colored according to the RMSF. Ribosomal proteins are emphasized.

The second representation is shown in Figure 4.10. The backbone atoms were sorted according to their position along the tunnel axis. To reduce the noise, a Gaussian filter with a standard deviation $\sigma = 4$ Å was applied. The standard deviation corresponds to the size of an amino acid [14].

The RMSF values vary along the tunnel axis. At the projected positions of the protein loops, the RMSF adopts hihger values, suggesting that the ribosomal pro-

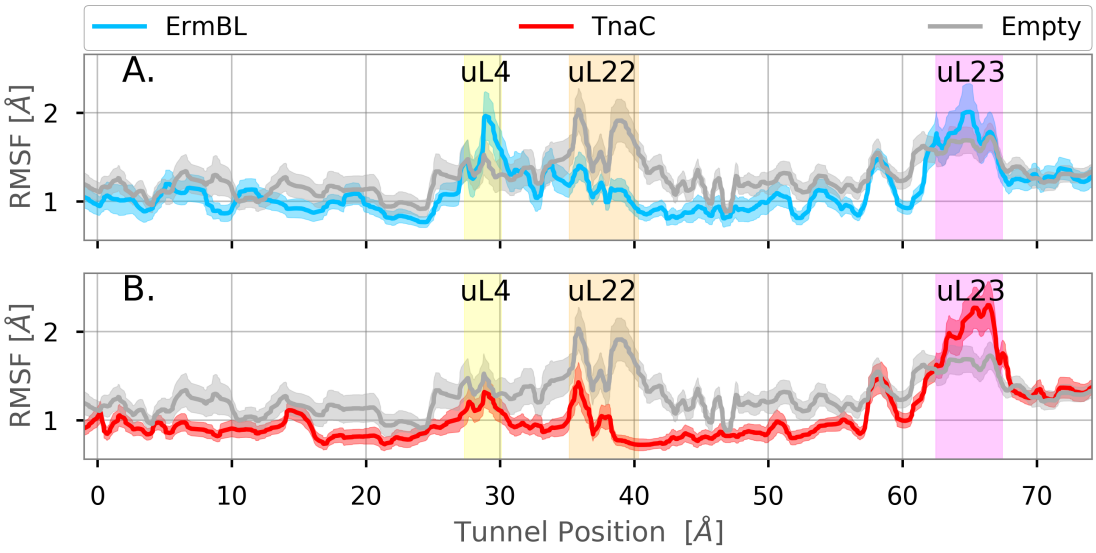

Figure 4.10: Shown is the backbone RMSF (solid line) averaged over the sub-ensembles. Both ensembles ErmBL (blue) and TnaC (red) are set in comparison to the ensemble Empty (grey). The error (filled curve) results from the standard error of the averaged RMSF. The backbone atoms were sorted along their position on the tunnel axis. The PTC is at position zero. The positions of the loops of the proteins uL4 (residues 62 to 64, yellow), uL22 (residues 89 to 92,orange) and uL23 (residues 70 to 74, magenta) are indicated by the vertical bars.

teins are more mobile than the rRNA. Compared to the empty tunnel (grey), the tunnels with ErmBL (blue line) and TnaC (red line) have a lower RMSF in most parts. The overall lower RMSF suggests that the nascent chains reduce the mobility of the exit tunnel.

The loops of the proteins seem to be especially affected by the presence of the nascent chains. In the case of the ErmBL peptide (Fig. 4.10, A) the RMSF of the uL4 loop (yellow) increases, while the RMSF of the the uL22 loop (orange) decreases. The loop of protein uL23 (magenta) seems to increase in the margin of error. In the case of the TnaC peptide (Fig. 4.10, B) the RMSF of the loops of the constriction site (uL4 and uL22) is reduced. But the loop of uL23 shows a higher RMSF.

To separate the contribution of the rRNA to the motion of the tunnel walls, the calculation of the RMSF was repeated while only considering the backbone atoms

of the rRNA.

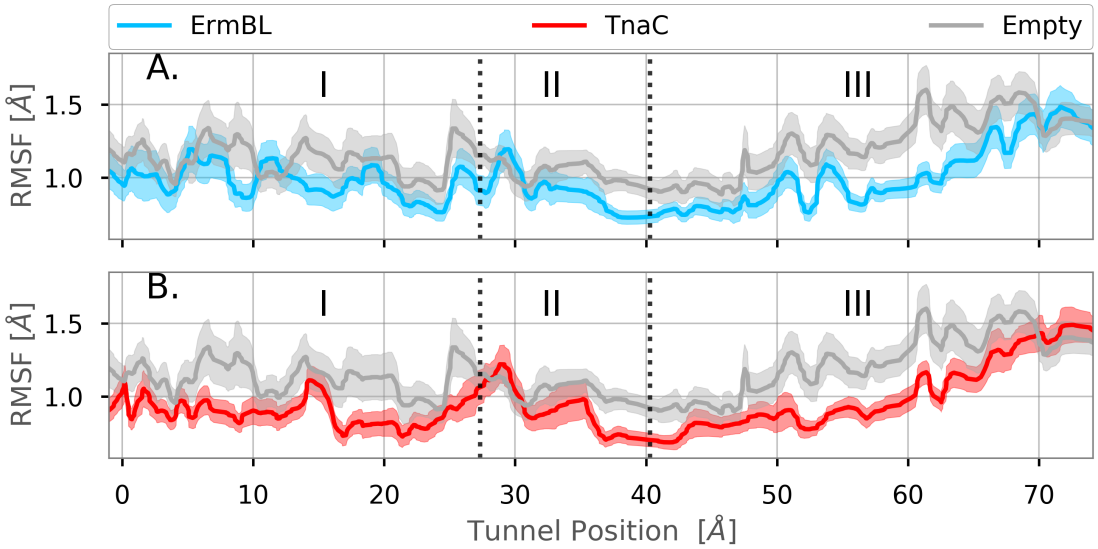

Figure 4.11: Projection of the RMSF of the rRNA backbone atoms averaged over the sub-ensembles. The ensembles ErmBL (blue) and TnaC (red) are set in comparison to the ensemble Empty (grey). The error (filled curve) results from the standard error of the averaged RMSF. The backbone atoms were sorted along their position along the tunnel axis. The PTC is at position zero. The tunnel was divided into three regions: pre-constriction site (I), constriction site (II) and post-constriction site (III).

The results are shown in Figure 4.11. The tunnel was separated into three parts. The first part consists of the atoms located in front of the constriction site (0 Å to 27 Å). The second part consists of the atoms located around the constriction site (27 Å to 41 Å). And the third part consists of the atoms located behind the constriction site (40 Å to 78 Å). The location of the constriction site was determined by the extrema of the positions of the residues of the loops of uL4 (residues 62 to 64) and uL22 (residues 89 to 92) projected on the tunnel axis.

The RMSF of the rRNA backbone varies along the tunnel axis. The lowest value of the RMSF is reached just behind the constriction site. The RMSF increases gradually over the third part. This increase is observed independently from the presence of the nascent chain. The RMSF is overall lower when a nascent chain is

present.

To assess whether the motion of the backbone atoms corresponds to a drift or a fluctuation, the RMSF was calculated after dividing the trajectories in two halves. The result is shown in Figure 4.12. Both curves show similar RMSF values for all three systems. Especially the proteins uL4 and uL23 yield different RMSF values.

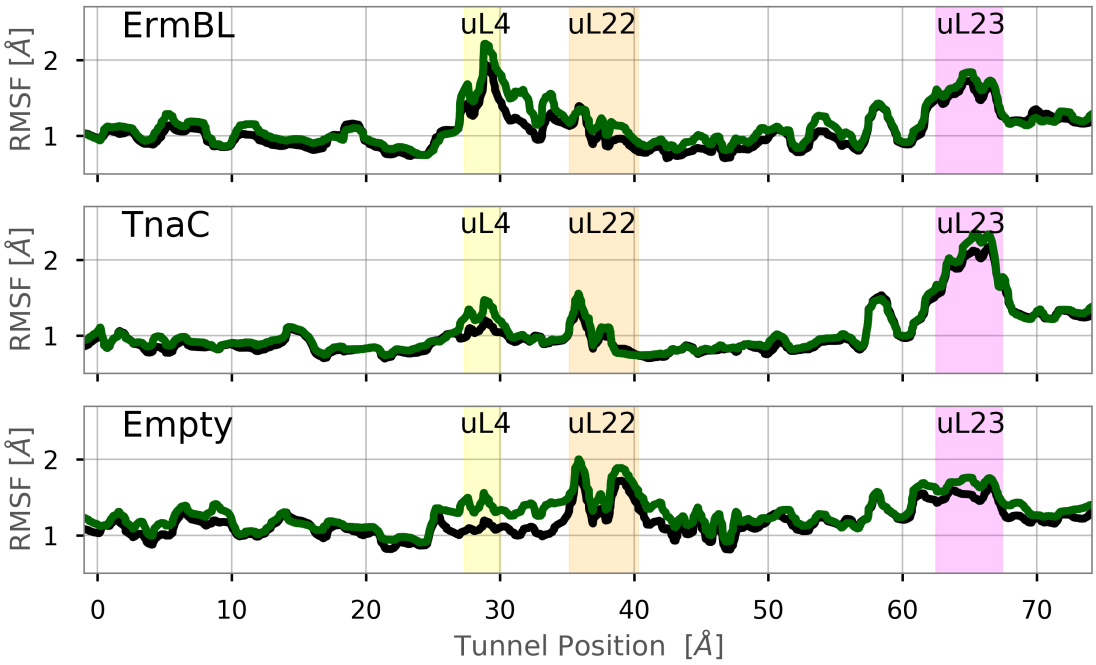

Figure 4.12: RMSF of the backbone atoms for ErmBL, TnaC and Empty ensembles. The trajectories corresponding to the ensembles were divided in two halves (first half: black line, second half: green line). The atoms were sorted along their position on the tunnel axis. The PTC is at position zero. The positions of the loops of the proteins uL4 (yellow), uL22 (orange) and uL23 (magenta) are indicated by vertical bars.

Differences in RMSF combined with increasing protein backbone RMSD (Fig. 4.3) suggest that the motion of the proteins is influenced by a small drift. Whereas minor differences in the RMSF regarding the rRNA together with a rather flat rRNA backbone RMSD (Fig. 4.3) suggest that the rRNA motion resembles a fluctuation.

The results of the backbone RMSF suggest the following. Ribosomal tunnel pro-

teins are more mobile than rRNA. The overall mobility decreases when a peptide is present. The loop of protein uL23 has an increased mobility with a peptide present. However, the motion of the proteins is partially influenced by a drift. Furthermore, the increase of the RMSF of the rRNA towards the exit suggest an increase of flexibility of the rRNA which is independent of a peptide.

5 Conclusions and Outlook

The previously mentioned studies (chapter 1) show that local interactions between the nascent chain and rRNA are essential for translational stalling [6, 35, 56, 58]. Additionally, ribosomal proteins contribute to stalling of SecM [31, 40, 56] and VemP [26, 54].

The conformational changes of the ribosomal exit tunnel presented in this thesis suggest that the exit tunnel is also globally affected by the presence of a nascent chain. These effects of the nascent chain on the dynamics of the ribosomal exit tunnel imply that a possible mechanism exists that controls peptide synthesis not only via local interactions, but globally.

Ribosomal proteins seem to contribute the most to conformational changes of the ribosomal exit tunnel. The dominant modes of motion were partially able to distinguish between conformations of the exit tunnel depending on the peptide. The extreme conformations of the exit tunnel indicate that the conformation of ribosomal proteins might depend on the peptide. If no peptide is present, the proteins seem to prefer a conformation which is radially closer to the tunnel axis and is pointing away from the exit. If ErmBL is present, the proteins seem to prefer a conformation which is radially further away from the tunnel axis and is pointing towards the exit. If TnaC is present, an additional slightly twisted conformation seems to be preferred.

Furthermore, ribosomal proteins were observed to be more mobile than rRNA. The mobility of the exit tunnel seems to be generally reduced if a peptide is present. Yet,

the loop of protein uL23 showed a possible increase in mobility. In the simulations, the mobility of protein loops was observed to be especially sensitive regarding the presence of a peptide. In addition, the flexibility of rRNA was observed to increase gradually behind the constriction site. This increase seems to be independent of the presence of a peptide.

A combination of three effects could influence the results.

First, drifts could influence the motion of the proteins. The seemingly preferred conformations of tunnel proteins might be influenced by insufficient sampling. Therefore, sampling has to be increased to support the conclusions regarding the conformations and monbility of ribosomal proteins.

Second, the simulations of the three different systems had different starting structures. To show more directly how the nascent chain affects the dynamics of the exit tunnel, the following approach could be applied. A simulation is started from a structure of an empty ribosome. After conformations of the empty ribosome are sampled, a nascent chain is inserted. After conformations of the ribosome with a nascent chain are sampled, the nascent chain is removed. The last two steps could be applied iteratively.

Third, the simulations were run at different temperatures. Although the temperature difference of 10 K does not seem to have an impact on the dynamics of the exit tunnel, a stronger conclusion could have been made if the systems were simulated at the same temperature.

The results of this study raise the following questions regarding the exit tunnel:

- Does the general decrease of mobility correlate with the type of the peptide?
- What mechanism causes the global decrease in flexibility of rRNA when a peptide is present?
- Does the increase of flexibility of the rRNA behind the constriction site have

a functional role?

This study investigated the effect of two peptides on the dynamics of the exit tunnel. Simulating the ribosome with other peptides, such as ErmCL, SecM or VemP would give more insight about the conformational dynamics of the exit tunnel and whether they depend on the type of the peptide.

Small conformational changes of or close to the PTC are responsible for stalling processes [57]. I speculate the mobility of the ribosomal exit tunnel might also be caused by small conformational changes in or around the PTC.

The diameter of the exit tunnel increases towards the exit [59]. The increased flexibility of the rRNA might be caused by this widening. A possible guiding mechanism for the emerging peptide could be the result of the increased flexibility of the rRNA.

Thus, further investigations regarding the conformational dynamics of the exit tunnel, especially the flexibility of the rRNA and its possible functional role are necessary.

Bibliography

[1]H. Abdi and L. J. Williams, "Principal component analysis", Wiley Interdisciplinary Reviews: Computational Statistics **2**, 433–459 (2010).

[2]R. Aduri, B. T. Psciuk, P. Saro, H. Taniga, H. B. Schlegel, and J. SantaLucia, "AMBER force field parameters for the naturally occurring modified nucleosides in RNA", Journal of Chemical Theory and Computation **3**, 1464–1475 (2007).

[3]R. K. Agrawal, M. R. Sharma, A. Yassin, I. Lahiri, and i. L. Spremulli, "Structure and function of organellar ribosomes as revealed by cryo-EM", in *Ribosomes* (Springer Vienna, Vienna, 2011), pp. 83–96.

[4]A. Amadei, A. B. M. Linssen, and H. J. C. Berendsen, "Essential dynamics of proteins", Proteins: Structure, Function, and Bioinformatics **17**, 412–425 (1993).

[5]S. Arenz, M. Abdelshahid, D. Sohmen, R. Payoe, A. L. Starosta, O. Berninghausen, V. Hauryliuk, R. Beckmann, and D. N. Wilson, "The stringent factor RelA adopts an open conformation on the ribosome to stimulate ppGpp synthesis", Nucleic Acids Research **44**, 6471–6481 (2016).

[6]S. Arenz, L. V. Bock, M. Graf, C. A. Innis, R. Beckmann, H. Grubmüller, A. C. Vaiana, and D. N. Wilson, "A combined cryo-EM and molecular dynamics approach reveals the mechanism of ErmBL-mediated translation arrest", Nature Communications **7**, 12026 (2016).

[7]N. Ban, R. Beckmann, J. H. D. Cate, J. D. Dinman, F. Dragon, S. R. Ellis, D. L. J. Lafontaine, L. Lindahl, A. Liljas, J. M. Lipton, M. A. McAlear, P. B. Moore, H. F. Noller, J. Ortega, V. G. Panse, V. Ramakrishnan, C. M. T. Spahn, T. A. Steitz, M. Tchorzewski, D. Tollervey, A. J. Warren, J. R. Williamson, D. Wilson, A. Yonath, and M. Yusupov, "A new system for naming ribosomal proteins", Current Opinion in Structural Biology **24**, 165–169 (2014).

[8]N. Ban, P. Nissen, J. Hansen, P. B. Moore, and T. A. Steitz, "The complete atomic structure of the large ribosomal subunit at 2.4 Å resolution", Science **289**, 905–920 (2000).

[9]H. J. C. Berendsen, J. R. Grigera, and T. P. Straatsma, "The missing term in effective pair potentials", The Journal of Physical Chemistry **91**, 6269–6271 (1987).

[10]H. J. C. Berendsen, J. P. M. Postma, W. F. van Gunsteren, A. DiNola, and J. R. Haak, "Molecular dynamics with coupling to an external bath", The Journal of Chemical Physics **81**, 3684–3690 (1984).

[11]H. Berman, K. Henrick, and H. Nakamura, "Announcing the worldwide Protein Data Bank", Nature Structural and Molecular Biology **10**, 980 (2003).

[12]L. Bischoff, O. Berninghausen, and R. Beckmann, "Molecular basis for the ribosome functioning as an L-tryptophan sensor", Cell Reports **9**, 469–475 (2014).

[13]G. Bussi, D. Donadio, and M. Parrinello, "Canonical sampling through velocity rescaling", Journal of Chemical Physics **126**, 014101 (2007).

[14]T. Creighton, *Proteins: Structures and molecular properties* (W.H. Freeman, 1992), p. 507.

[15]L. R. Cruz-Vera, S. Rajagopal, C. Squires, and C. Yanofsky, "Features of ribosome-peptidyl-tRNA interactions essential for tryptophan induction of tna operon expression", Molecular Cell **19**, 333–343 (2005).

[16]U. Essmann, L. Perera, M. L. Berkowitz, T. Darden, H. Lee, and L. G. Pedersen, "A smooth particle mesh Ewald method", The Journal of Chemical Physics **103**, 8577–8593 (1995).

[17]N. Fischer, P. Neumann, A. L. Konevega, L. V. Bock, R. Ficner, M. V. Rodnina, and H. Stark, "Structure of the E. coli ribosome-EF-Tu complex at <3 Å resolution by C_S-corrected cryo-EM", Nature **520**, 567–570 (2015).

[18]F. Franks, *Water*, 2nd ed. (Royal Society of Chemistry, Cambridge, 2000).

[19]R. Green and and H. F. Noller, "Ribosomes and Translation", Annual Review of Biochemistry **66**, 679–716 (1997).

[20]P. Gupta, B. Liu, D. Klepacki, V. Gupta, K. Schulten, A. S. Mankin, and N. Vázquez-Laslop, "Nascent peptide assists the ribosome in recognizing chemically distinct small molecules", Nature Chemical Biology **12**, 153–158 (2016).

[21]B. Hess, "Convergence of sampling in protein simulations", Physical Review E - Statistical, Nonlinear, and Soft Matter Physics **65** (2002) `10.1103/PhysRevE.65.031910`.

[22]B. Hess, "P-LINCS: A parallel linear constraint solver for molecular simulation", Journal of Chemical Theory and Computation **4**, 116–122 (2008).

[23]B. K. Ho and F. Gruswitz, "HOLLOW: Generating Accurate Representations of Channel and Interior Surfaces in Molecular Structures", BMC Structural Biology **8**, 49 (2008).

[24]F. G. Hopkins and S. W. Cole, "A contribution to the chemistry of proteid. Part II . The constitution of tryptophanase and the action of bacteria upon it", J Physiol **29**, 451–466 (1903).

[25]V. Hornak, R. Abel, A. Okur, B. Strockbine, A. Roitberg, and C. Simmerling, "Comparison of multiple amber force fields and development of improved protein backbone parameters", Proteins: Structure, Function and Genetics **65**, 712–725 (2006).

[26]E. Ishii, S. Chiba, N. Hashimoto, S. Kojima, M. Homma, K. Ito, Y. Akiyama, and H. Mori, "Correction for Ishii et al., Nascent chain-monitored remodeling of the Sec machinery for salinity adaptation of marine bacteria", Proceedings of the National Academy of Sciences **112**, 201522482 (2015).

[27]K. Ito and S. Chiba, "Arrest Peptides: *Cis* -Acting Modulators of Translation", Annual Review of Biochemistry **82**, 171–202 (2013).

[28]N. R. James, A. Brown, Y. Gordiyenko, and V. Ramakrishnan, "Translational termination without a stop codon", Science **354**, 1437–1440 (2016).

[29]I. S. Joung and T. E. Cheatham, "Determination of alkali and halide monovalent ion parameters for use in explicitly solvated biomolecular simulations", Journal of Physical Chemistry B **112**, 9020–9041 (2008).

[30]D. J. Klein, P. B. Moore, and T. A. Steitz, "The roles of ribosomal proteins in the structure assembly, and evolution of the large ribosomal subunit", Journal of Molecular Biology **340**, 141–177 (2004).

[31]M. G. Lawrence, L. Lindahl, and J. M. Zengel, "Effects on translation pausing of alterations in protein and RNA components of the ribosome exit tunnel", Journal of Bacteriology **190**, 5862–5869 (2008).

[32]L. Lins, A. Thomas, and R. Brasseur, "Analysis of accessible surface of residues in proteins", Protein Science **12**, 1406–1417 (2003).

[33]A. B. Loveland, G. Demo, N. Grigorieff, and A. A. Korostelev, "Ensemble cryo-EM elucidates the mechanism of translation fidelity", Nature **546**, 113–117 (2017).

[34]J. Lu and C. Deutsch, "Electrostatics in the Ribosomal Tunnel Modulate Chain Elongation Rates", Journal of Molecular Biology **384**, 73–86 (2008).

[35]G. I. Makarov, A. V. Golovin, N. V. Sumbatyan, and A. A. Bogdanov, "Molecular dynamics investigation of a mechanism of allosteric signal transmission in ribosomes", Biochemistry (Moscow) **80**, 1047–1056 (2015).

[36]A. K. Martínez, E. Gordon, A. Sengupta, N. Shirole, D. Klepacki, B. Martinez-Garriga, L. M. Brown, M. Benedik, C. Yanofsky, A. S. Mankin, N. Vazquez-Laslop, M. S. Sachs, and L. R. Cruz-Vera, "Interactions of the TnaC nascent peptide with rRNA in the exit tunnel enable the ribosome to respond to free tryptophan", Nucleic Acids Research **42**, 1245–1256 (2014).

[37]P. McNicholas, R. Salavati, and D. Oliver, "Dual regulation of Escherichia coli secA translation by distinct upstream elements.", Journal of molecular biology **265**, 128–141 (1997).

[38]R. A. Milligan and P. N. Unwin, "In vitro crystallization of ribosomes from chick embryos", Journal of Cell Biology **95**, 648–653 (1982).

[39]H. Nakatogawa and K. Ito, "Secretion monitor, secM, undergoes self-translation arrest in the cytosol", Molecular Cell **7**, 185–192 (2001).

[40]H. Nakatogawa and K. Ito, "The ribosomal exit tunnel functions as a discriminating gate", Cell **108**, 629–636 (2002).

[41]K. H. Nierhaus and D. N. Wilson, *Protein Synthesis and Ribosome Structure: Translating the Genome* (Wiley-VCH, 2004), p. 579.

[42]P. Nissen, "The Structural Basis of Ribosome Activity in Peptide Bond Synthesis", Science **289**, 920–930 (2000).

[43]J. Noeske, J. Huang, N. B. Olivier, R. A. Giacobbe, M. Zambrowski, and J. H. D. Cate, "Synergy of streptogramin antibiotics occurs independently of their effects on translation", Antimicrobial Agents and Chemotherapy **58**, 5269–5279 (2014).

[44]J. Noeske, M. R. Wasserman, D. S. Terry, R. B. Altman, S. C. Blanchard, and J. H. D. Cate, "High-resolution structure of the Escherichia coli ribosome", Nature Structural and Molecular Biology **22**, 336–341 (2015).

[45]H. F. Noller, V. Hoffarth, and L. Zimniak, "Unusual resistence of peptidyl transferase to protein extraction procedures", Science **256**, 1416–1419 (1992).

[46]G. E. Palade, "a Small Particulate Component of the Cytoplasm", The Journal of Cell Biology **1**, 59–68 (1955).

[47]M. Parrinello and A. Rahman, "Polymorphic Transitions in Alkali Halides, a Molecular Dynamics Study", Le Journal de Physique Colloques **42**, C6–511–C6–515 (1981).

[48]P. A. Penczek, "Image restoration in cryo-electron microscopy", Methods in Enzymology **482**, 35–72 (2010).

[49]A. Pérez, I. Marchán, D. Svozil, J. Sponer, T. E. Cheatham, C. A. Laughton, and M. Orozco, "Refinement of the AMBER Force Field for Nucleic Acids: Improving the Description of α/γ Conformers", Biophysical Journal **92**, 3817–3829 (2007).

[50]S. Pronk, S. Páll, R. Schulz, P. Larsson, P. Bjelkmar, R. Apostolov, M. R. Shirts, J. C. Smith, P. M. Kasson, D. Van Der Spoel, B. Hess, and E. Lindahl, "GROMACS 4.5: A high-throughput and highly parallel open source molecular simulation toolkit", Bioinformatics **29**, 845–854 (2013).

[51]H. J. Rheinberger, H. Sternbach, and K. H. Nierhaus, "Three tRNA binding sites on Escherichia coli ribosomes", Proceedings of the National Academy of Sciences **78**, 5310 (1981).

[52]B. Seidelt, C. A. Innis, D. N. Wilson, M. Gartmann, J.-P. Armache, E. Villa, L. G. Trabuco, T. Becker, T. Mielke, K. Schulten, T. A. Steitz, and R. Beckmann, "Structural Insight into Nascent Polypeptide Chain-Mediated Translational Stalling", Science **326**, 1412–1415 (2009).

[53]F. H. Stillinger and A. Rahman, "Improved simulation of liquid water by molecular dynamics", The Journal of Chemical Physics **60**, 1545–1557 (1974).

[54]T. Su, J. Cheng, D. Sohmen, R. Hedman, O. Berninghausen, G. von Heijne, D. N. Wilson, and R. Beckmann, "The force-sensing peptide VemP employs extreme compaction and secondary structure formation to induce ribosomal stalling", eLife **6**, 1–17 (2017).

[55]K. N. Trueblood, H. B. Bürgi, H. Burzlaff, J. D. Dunitz, C. M. Gramaccioli, H. H. Schulz, U. Shmueli, and S. C. Abrahams, "Atomic Dispacement Parameter Nomenclature. Report of a Subcommittee on Atomic Displacement Parameter Nomenclature", Acta Crystallographica Section A Foundations of Crystallography **52**, 770–781 (1996).

[56]N. Vázquez-Laslop, H. Ramu, D. Klepacki, K. Kannan, and A. S. Mankin, "The key function of a conserved and modified rRNA residue in the ribosomal response to the nascent peptide", EMBO Journal **29**, 3108–3117 (2010).

[57]N. Vázquez-laslop, H. Ramu, and A. Mankin, "Nascent peptide-mediated ribosome stalling promoted by antibiotics", in *Ribosomes structure, function, and dynamics* (Springer Vienna, Vienna, 2011), pp. 377–392.

[58]N. Vazquez-Laslop, C. Thum, and A. S. Mankin, "Molecular Mechanism of Drug-Dependent Ribosome Stalling", Molecular Cell **30**, 190–202 (2008).

[59]N. R. Voss, M. Gerstein, T. A. Steitz, and P. B. Moore, "The Geometry of the Ribosomal Polypeptide Exit Tunnel", Journal of Molecular Biology **360**, 893–906 (2006).

[60]J. D. Watson, "Involvement of RNA in the Synthesis of Proteins: The ordered interaction of three classes of RNA controls the assembly of amino acids into proteins", Science **140**, 17–26 (1963).

[61]D. N. Wilson, "Peptides in the Ribosomal Tunnel Talk Back", Molecular Cell **41**, 247–248 (2011).

[62]J. Zhang, X. Pan, K. Yan, S. Sun, N. Gao, and S. F. Sui, "Mechanisms of ribosome stalling by SecM at multiple elongation steps", eLife **4**, e09684 (2015).

Acknowledgments

I am sincerely grateful for the helpful discussions, guidance and support from Helmut Grubmüller and the department members during my stay at the Max Planck Institute for Biophysical Chemistry. Special thanks go to Lars V. Bock, Michal H. Kolář and Andrea Vaiana, who provided me with helpful advice and animated discussions when needed.

Erklärung nach §18(8) der Prüfungsordnung für den Bachelor-Studiengang Physik und den Master-Studiengang Physik an der Universität Göttingen:

Hiermit erkläre ich, dass ich diese Abschlussarbeit selbständig verfasst habe, keine anderen als die angegebenen Quellen und Hilfsmittel benutzt habe und alle Stellen, die wörtlich oder sinngemäß aus veröffentlichten Schriften entnommen wurden, als solche kenntlich gemacht habe.
Darüberhinaus erkläre ich, dass diese Abschlussarbeit nicht, auch nicht auszugsweise, im Rahmen einer nichtbestandenen Prüfung an dieser oder einer anderen Hochschule eingereicht wurde.

Göttingen, den 5. Dezember 2017

(Vitali Telezki)